Università Politecnica delle Marche
Scuola di Dottorato di Ricerca in Ingegneria Civile, Ambientale, Edile e Architettura
Curriculum in Ingegneria Civile-Ambientale, Edile e Architettura

Advanced Geomatic Techniques in support of Monitoring and Management in Thematic GIS

Ph.D. Dissertation of:
Fabio Piccinini

Advisor:
Prof. Eva Savina Malinverni

Curriculum Supervisor:
Prof. Francesco Fatone

XXXIV edition - new series

Università Politecnica delle Marche
Scuola di Dottorato di Ricerca in Ingegneria Civile, Ambientale, Edile e Architettura
Curriculum in Ingegneria Civile-Ambientale, Edile e Architettura

Advanced Geomatic Techniques in support of Monitoring and Management in Thematic GIS

Ph.D. Dissertation of:
Fabio Piccinini

Advisor:
Prof. Eva Savina Malinverni

Curriculum Supervisor:
Prof. Francesco Fatone

XXXIV edition - new series

Università Politecnica delle Marche
Scuola di Dottorato di Ricerca in Ingegneria Civile, Ambientale, Edile e Architettura
Facoltà di Ingegneria
Via Brecce Bianche – 60131 Ancona (AN), Italy

Acknowledgments

This thesis is the result of a PhD co-funded by Flyengineering s.r.l., within the framework of the Marche Region "Eureka - borse di studio per dottorato di ricerca per l'innovazione" (Eureka - PhD scholarships for innovation).

Firstly, I would like to express my sincere gratitude to Prof. Eva Savina Malinverni, my advisor and academic tutor, to Mrs. Vania Feliziani, my company tutor, and to Dr. Roberto Pierdicca and Mr. Samuele Crucianelli, who have always been a great support to me in the different activities.

A special thanks also goes to Prof. Luis Javier Sánchez Aparicio of the Higher Technical School of Architecture of Madrid, with whom I had the opportunity to collaborate online.

I would also like to thank all my coworkers in both the GAP (Geomatics Applications & Processing) research group and Flyengineering, with whom I shared good times both at work and in leisure.

Finally, I would like to thank my family and friends who, as always, have been a great companion and support.

Ancona, February 2022

Fabio Piccinini

Sommario

Nel campo della Geomatica, esistono numerosi strumenti e tecniche che vengono utilizzati a seconda delle caratteristiche dell'oggetto del rilievo. Nella maggior parte dei casi si utilizza una combinazione di essi per sfruttare al meglio le loro capacità in relazione allo scopo del rilievo, dovendo quindi lavorare con diversi tipi di dati provenienti da diverse fonti.

L'uso dei GIS (Geographical Information Systems) consente di integrare questi dati in un geo-database e di metterli in relazione tra loro spazialmente, temporalmente e semanticamente per ulteriori elaborazioni. Le applicazioni GIS permettono anche la produzione di mappe personalizzate per una visualizzazione ottimale dei dati, fornendo un buon supporto decisionale. Essi consentono una completa analisi di qualsiasi informazione che coinvolge componenti spazio-temporali. Infatti, è noto che la tecnologia GIS ha una vasta gamma di applicazioni nella gestione di qualsiasi tipo di risorsa che può essere descritta su scala geografica. Inoltre, rappresenta uno strumento essenziale per il processo decisionale, quando si devono gestire dati eterogenei nei medesimi fenomeni.

Di fatto, le caratteristiche dei GIS sono state ampiamente adottate in molti campi di applicazione, compresi la gestione delle risorse energetiche, crescita urbana e popolazione, applicazioni di Land Cover/Land Use, patrimonio culturale e archeologia.

In questa tesi di dottorato è stato introdotto l'uso di applicazioni GIS in due flussi di lavoro riguardanti due diversi domini: le ispezioni termografiche aeree da UAV (Unmanned Aerial Vehicle) di impianti fotovoltaici (PV) e i rilievi di edifici, quartieri o interi territori, combinando Terrestrial Laser Scanning (TLS) e fotogrammetria aerea da UAV.

Il settore del fotovoltaico è cresciuto sia in termini di impianti installati che di energia prodotta e, negli ultimi due decenni, c'è stato un notevole aumento della potenza fotovoltaica installata su tutto il territorio italiano che oggi rappresenta un'importante fonte di energia per il paese e una delle componenti più importanti nella produzione di energia pulita e rinnovabile. È quindi emersa la necessità di mantenere questi impianti nella loro massima efficienza durante tutto il loro ciclo di vita, per beneficiarne sia dal punto di vista ecologico che economico.

Anche se oggi sono disponibili diverse tecniche per l'ispezione dei pannelli

solari (la maggior parte delle quali semi-automatiche), la gestione è ancora basata sul lavoro manuale.

La comunità dei ricercatori si sta concentrando principalmente sulla scoperta di nuovi modi per il rilevamento automatico dei guasti negli impianti fotovoltaici, soprattutto attraverso l'uso di sistemi di intelligenza artificiale.

Un'altra importante missione è quella di definire uno standard (o protocollo) per gestire la complessa quantità di informazioni che proviene da un impianto fotovoltaico attivo.

Un forte contributo per una filiera più affidabile e economica di O&M (Operations and Maintenance) è rappresentato dall'adozione di Sistemi Informativi Geografici (GIS).

Generalmente, le informazioni sugli impianti fotovoltaici non sono strutturate, e i proprietari di tali impianti hanno bisogno di rapporti specifici che forniscano informazioni sullo stato dell'impianto stesso. Al fine di ridurre questi sforzi e facilitare la gestione, è necessario introdurre un sistema informativo nella filiera della gestione degli impianti fotovoltaici che sia in grado di raccogliere e organizzare tutte le informazioni sugli stessi e sui risultati delle ispezioni (come il numero totale di moduli, la loro dimensione, il numero di celle, i nomi dei produttori e dei prodotti, la produzione effettiva di energia, i guasti, le informazioni spazio-temporali e le operazioni di manutenzione effettuate).

Nel campo della gestione dei dati dei progetti urbani ed edilizi, l'uso di software di modellazione tridimensionale (3D) e di piattaforme open-source è diventato sempre più frequente negli ultimi anni. Le normative in costante aggiornamento suggeriscono e, in alcuni casi, impongono l'adozione di nuovi sistemi informativi digitali sostenibili, avanzati e più accessibili.

La piattaforma GIS si adatta bene alla gestione dei dati alla scala urbana in una determinata area geografica. Un GIS 3D può essere utilizzato come mappa 3D di riferimento per qualsiasi attività di gestione della pianificazione urbana e tra queste anche in caso di emergenza sismica. In particolare, il GIS è suggerito come uno strumento adatto per la mappatura del rischio, per comprendere meglio l'estensione spaziale del rischio e per documentare gli effetti delle situazioni di pericolo, secondo l'ISO/IEC 31010:2009 e le Raccomandazioni per la valutazione del rischio nazionale.

Per quanto riguarda le ispezioni termografiche da UAV di impianti fotovoltaici, introducendo l'uso dei GIS nel flusso di lavoro, l'obiettivo è quello di contribuire a definire una pipeline di lavoro dall'acquisizione dei dati alla creazione di report, e di proporre una struttura dati "standard" per qualsiasi impianto che permetta la creazione automatica di report e query. Questo approccio è particolarmente utile nei grandi impianti. Le applicazioni GIS permettono l'organizzazione di un database geo-referenziato dell'impianto, questo può aiutare i manutentori, i proprietari e i finanziatori a supervisionare e lo-

calizzare i moduli fotovoltaici danneggiati e monitorare la loro evoluzione e l'impatto sulle condizioni di lavoro dell'impianto.

Relativamente ai rilievi fotogrammetrici e TLS urbani di edifici, quartieri o interi territori, il GIS è stato introdotto con l'obiettivo di integrare i dati ottenuti dalle varie fonti in un geo-database che permette ulteriori elaborazioni grazie alla loro relazione spaziale.

L'integrazione dei linguaggi di programmazione nei GIS, come Python in QGIS (Quantum GIS), permette anche lo sviluppo di flussi di lavoro automatizzati e personalizzati. Infatti, uno degli obiettivi perseguiti in questa tesi è stato quello di automatizzare l'estrazione di informazioni relative a caratteristiche geometriche specifiche degli edifici, che sono anche frequentemente utilizzate come dati di input per una valutazione speditiva dell'indice di vulnerabilità sismica.

Questa tesi è il risultato di un dottorato cofinanziato da Flyengineering s.r.l., nell'ambito del progetto "Eureka - borse di studio per dottorato di ricerca per l'innovazione" della regione Marche. L'obiettivo di questo progetto è quello di promuovere e connettere la ricerca accademica con il tessuto economico regionale, al fine di promuovere l'innovazione e rafforzare la competitività delle imprese che operano nella regione e contribuire ad aumentare l'occupabilità dei soggetti con elevato livello di istruzione.

Abstract

In the field of Geomatics, there are numerous tools and techniques that are used depending on the characteristics of the survey object. In most cases a combination of them is used to best exploit their capabilities in relation to the purpose of the survey, having to work with different data types from different sources.

The use of Geographical Information Systems (GIS) allows to integrate these data in a geo-database and to relate them to each other spatially, temporally and semantically for further processing. GIS applications also permit the production of custom maps for an optimal data visualisation, providing a good decision support. They allow a complete breakdown over any information that involves spatio-temporal components. In fact, it is well known that GIS technology has a wide field of applications in the management of any kind of resource that can be described at geographical scale. It represents an essential tool for the decision-making process, when heterogeneous data have to be managed in the same phenomena.

Indeed, GIS features have been widely adopted in many application fields, including energy resource management, urban growth and population, land cover/land use applications, cultural heritage and archaeology.

In this PhD thesis the use of GIS applications has been introduced in two workflows concerning two different domains: the UAV (Unmanned Aerial Vehicle) thermographic inspections of photovoltaic (PV) plants and the urban surveys of buildings, districts, or entire villages, combining Terrestrial Laser Scanning (TLS) and aerial photogrammetry using UAV.

The photovoltaic sector grew up both in terms of installed plants and energy produced and, in the last two decades, there was a considerable increase in installed PV power throughout the Italian territory that now represent an important source of energy for the country and one of the most important components in the production of clean and renewable energy. Therefore, emerged the need to maintain these plants in their maximum efficiency during their whole lifecycle, to benefit from both the ecologic and the economic point of view.

Although several techniques are nowadays available for the inspection of solar panels (most of them semi-automatic), the management is still based on handywork.

The research community is mainly focusing on uncovering new ways for the automatic detection of faults in PV plants, especially through the use of artificial intelligence systems.

Another important mission is to define a standard (or protocol) to manage the complex amount of information that comes from an active PV plant.

A strong contribution for a more reliable and affordable pipeline of O&M (Operations and Maintenance) is represented by the adoption of Geographical Information Systems (GIS).

Indeed, the information about PV plants is generally not structured, and the owners of such systems need specific reports that provide information about the status of the system itself. In order to reduce these efforts and facilitate management, it is necessary to introduce an information system in the pipeline of PV plants management that is able to collect and organize the whole information about the solar power plants and their inspections results (such as modules total number, their size, number of cells, manufacturers and product names, effective power production, faults, spatio-temporal information, and maintenance operations carried out).

In the field of data management of urban and building projects, the use of three-dimensional (3D) modelling software and open-source platforms has become increasingly frequent in recent years. The constantly updated regulations suggest and, in some cases, enforce the adoption of new sustainable, advanced and more accessible digital information systems.

The GIS platform is well suited for data management at the urban scale in a given geographical area. A 3D GIS can be used as a reference 3D map for any urban planning management activities and among them also in case of seismic emergency. In particular, GIS is suggested as a suitable tool for the risk mapping, for better understand the spatial extent of risk and to document the effects of hazard situations, according to the ISO/IEC 31010:2009 and the Recommendations for National Risk Assessment.

Regarding UAV thermographic inspections of photovoltaic installations, introducing the use of GIS into the workflow, the aim is to contribute to define a pipeline of work from data acquisition to the report creation, and to propose a "standard" data structure for any system that permits automatic report creation and query. This approach is particularly valuable in large plants. GIS applications allow the organization of a geo-referenced database of the system, this can help maintainers, owners, and promoters to supervise and locate damaged PV modules and monitor their evolution and impact on plant working conditions.

Concerning the photogrammetric and TLS urban surveys of buildings, districts or entire territories, the GIS has been introduced with the objective of integrating the data obtained from the various sources in a geo-database allow-

ing further processing thanks to their spatial relation.

The integration of programming languages in GIS, such as Python in QGIS (Quantum GIS), also allows the development of automated and customised workflows. In fact, one of the objectives pursued in this thesis was to automate the extraction of information related to specific geometrical characteristics of the buildings, which are also frequently used as input data for a preliminary assessment of the seismic vulnerability index.

This thesis is the result of a PhD co-funded by Flyengineering s.r.l., within the framework of the Marche Region "Eureka - borse di studio per dottorato di ricerca per l'innovazione" (Eureka - PhD scholarships for innovation). The aim of this project is to promote and link academic research with the regional economic scene, in order to promote innovation and strengthen the competitiveness of companies operating in the region and to help increase the employability of highly educated people.

Contents

List of Figures

List of Tables

Chapter 1

Introduction

1.1 Context

In the field of Geomatics, there are numerous tools and techniques that are used depending on the characteristics of the survey object. In most cases a combination of them is used to best exploit their capabilities in relation to the purpose of the survey, having to work with different data types from different sources.

The use of Geographical Information Systems (GIS) allows to integrate the data from the various sources in a geo-database and to relate them to each other spatially, temporally and semantically for further processing. GIS applications also permit the production of custom maps for an optimal data visualisation, providing a good decision support. They allow a complete breakdown over any information that involves spatio-temporal components. In fact, it is well known that GIS technology has a wide field of applications in the management of any kind of resource that can be described at geographical scale. It represents an essential tool for the decision-making process, when heterogeneous data have to be managed in the same phenomena [1].

Indeed, GIS features have been widely adopted in many application fields, including energy resource management [2], urban growth and population [3], land cover/land use applications [4], cultural heritage and archaeology [5].

In this PhD thesis the use of GIS applications has been introduced in two workflows concerning two different domains: the UAV (Unmanned Aerial Vehicle) thermographic inspections of photovoltaic (PV) plants and the urban surveys of buildings, districts, or entire villages, combining Terrestrial Laser Scanning (TLS) and UAV photogrammetry.

Renewable energy sources represent one of the main ways to reduce fossil fuel usage and the consequent pollution; therefore, European and worldwide countries had heavily invested for stimulate the use of clean energy. As a result, the photovoltaic sector grew up both in terms of installed plants and energy produced and, in the last two decades, there was a considerable increase in installed PV power throughout the Italian territory that now represent an

important source of energy for the country [6] and one of the most important components in the production of clean and renewable energy [7, 8].

Therefore, emerged the need to maintain these plants in their maximum efficiency during their whole lifecycle, to benefit from both the ecologic and the economic point of view [9].

Nevertheless, this work of maintaining the operational status of a PV plant at its best performances is not trivial and requires many efforts, both on-site and office. Although several techniques are nowadays available for the inspection of solar panels (most of them semi-automatic), the management is still based on handywork [10, 11].

The research community is mainly focusing on uncovering new ways for the automatic detection of faults in PV plants, especially through the use of artificial intelligence systems [12].

Another important mission is to define a standard (or protocol) to manage the complex amount of information that comes from an active PV plant.

The operation and maintenance (O&M) of a PV power plant is of extreme importance to guarantee its optimal performance [13]. A strong contribution for a more reliable and affordable pipeline of O&M is represented by the adoption of Geographical Information Systems (GIS).

Indeed, the information about PV plants is generally not structured, and the owners of such systems need specific reports that provide information about the status of the system itself. In order to reduce these efforts and facilitate management, it is necessary to introduce an information system in the pipeline of PV plants management that is able to collect and organize the whole information about the solar power plants and their inspections results (such as modules total number, their size, number of cells, manufacturers and product names, effective power production, faults, spatio-temporal information, and maintenance operations carried out). As stated, the potential of the utilization of GIS based methodologies in the energy field seems to be of great interest in the near future [1].

In the field of data management of urban and building projects, the use of three-dimensional (3D) modelling software and open-source platforms has become increasingly frequent in recent years. The constantly updated regulations suggest and, in some cases, enforce the adoption of new sustainable, advanced and more accessible digital information systems [14, 15]. This smart approach is not only intended to represent optimal management of the data of one or more projects after a seismic event, but it also serves to define preventive measures (real-time data visualisation, disasters prediction, etc.) that can be taken to deal with this type of emergency [16].

The GIS platform is well suited for data management at the urban scale in a given geographical area. Moreover, 3D GIS software gives a three-dimensional

model of the topographic representation of the terrain with the geolocalization of the buildings in the form of volumes at the various LODs (Level of Details) [17].

A 3D GIS can be used as a reference 3D map for any urban planning management activities and among them also in case of seismic emergency [18]. In particular, GIS is suggested as a suitable tool for the risk mapping, for better understand the spatial extent of risk and to document the effects of hazard situations, according to the ISO/IEC 31010:2009 and the Recommendations for National Risk Assessment [19].

1.2 Objectives and main contributions

Regarding UAV thermographic inspections of photovoltaic installations, introducing the use of GIS into the workflow, the aim is to contribute to define a pipeline of work from data acquisition to the report creation, and to propose a "standard" data structure for any system that permits automatic report creation and query; the purpose is to extend the GIS implementation in PV systems management, from the building location optimization, to the operation and maintenance topic as well. This approach is particularly valuable in large plants.

Indeed, it is a common practice used by companies dealing with O&M of PV plants, to create technical reports about the health status of the plants. This operation is, nowadays, made manually; this activity is very time consuming and error prone. GIS applications allow the organization of a geo-referenced database of the system, this can help maintainers, owners, and promoters to supervise and locate damaged PV modules and monitor their evolution and impact on plant working conditions.

The main contributions of this thesis in the field of PV system management can therefore be summarised as:

- The definition of a *standard pipeline* for the PV plants O&M within a GIS environment.
- The definition of a *conceptual model*, for the management of heterogeneous information in a GIS environment, generalized for any PV plant.
- The adoption of an *open source* GIS environment for the *automatic production of reports*, which can have a positive impact for companies dealing with PV plants management.

Concerning the photogrammetric and TLS urban surveys of buildings, districts or entire territories, the GIS has been introduced with the objective of

integrating the data obtained from the various sources in a geo-database allowing further processing thanks to their spatial relation.

The main contribution of the thesis in this field concern the automation of the extraction of information related to specific characteristics of the buildings, which are also frequently used as input data for a preliminary assessment of the seismic vulnerability index, achieved through the development of automated and customised workflows allowed by the integration of Python[1] in QGIS[2] (Quantum GIS).

This thesis is the result of a PhD co-funded by Flyengineering s.r.l., within the framework of the Marche Region "Eureka - borse di studio per dottorato di ricerca per l'innovazione" (Eureka - PhD scholarships for innovation). The aim of this project is to promote and link academic research with the regional economic scene, in order to promote innovation and strengthen the competitiveness of companies operating in the region and to help increase the employability of highly educated people.

Therefore, given the nature of the Eureka project, the underlying objective is to extend and enhance Flyengineering's products and services by providing them with the knowledge of innovative tools and techniques in the field of geomatics.

1.3 Structure of the thesis

The thesis is structured in six chapters, which are described below.

This first chapter provided a description of the context that motivated the realisation of this thesis and its main objectives and contributions.

Chapter 2 will illustrate the state of the art regarding the use of GIS in the two application domains.

Chapter 3 will describe the followed pipelines with their respective data acquisition and processing steps, detailing the structure of the relational geodatabase for the management of photovoltaic systems and the algorithms written in Python for the automatic computation of parameters concerning the geometric characteristics of buildings, while presenting the case studies used to test them.

Chapter 4 will present the results obtained following the procedures described in Chapter 3, which will then be discussed in Chapter 5.

Chapter 6 aims to highlight some possible improvements and future developments that could build on this work.

[1] `https://www.python.org/`
[2] `https://www.qgis.org/`

Chapter 2

State of the art about the use of Geographic Information Systems

In this chapter the state of the art regarding the use of GIS in the two application domains discussed in this thesis will be presented.

2.1 Use of GIS in the Photovoltaic domain

Regarding the use of GIS in the application domain of photovoltaic systems, several interesting works have been found in the literature. In [20] the authors present a GIS based technique to estimate PV production considering the shadowing effect; in another work [21] the GIS potential is exploited to create virtual dynamic maps of a power plant, including georeferenced thermal images. Moreover, the same authors have used GIS together with Global Positioning Systems (GPS) and Unmanned Aerial Vehicles (UAV) to propose an efficient inspection and maintenance of PV power plants, where they also developed different functions to perform query and investigations over the effective state of conservation of PV plants [22].

GIS, as is well known, is able to manage different data coming from more sources, and permit to infer information by performing correlation among the same data. In [23], the designed tool has proven to be useful to analyze the effects of faults on a PV field and the most common PV defect locations and correlations. The study highlighted that such correlations are more reliable when applied to a huge PV plant, with respect to smaller ones.

It is very interesting to note that an extensive use of GIS to perform forecasting and estimations for the optimization of landscape and urban resources emerged from the literature.

For example, in [24], the study demonstrates that is possible to efficiently arrange solar power by understanding the amount of solar radiation, to figure out the land and roof suitability for solar power. The purpose was to achieve the promotion of the aggressive utilization of agricultural land and roofs that have not been used to grasp the efficient land and roofs for PV generation units.

In other studies, geographical and morphological variables have been taken into account with the same purpose: identifying suitable locations for the construction of solar farms, as it requires detailed information and accurate planning. To this end, solar radiation [25], urban roofs information [26] and Digital Elevation Models [25] have been used for optimizing the installation of PV plants, considering inclination, orientation, morphology [27, 28, 29, 30].

As evidence that GIS is probably a good solution to manage such a complex domain, the European Union (EU) community have published the PVGIS [31], an open access system for accessing PV information all over Europe, including:

- PV potential for different technologies and configurations of grid connected and standalone systems.
- Solar radiation and temperature, as monthly averages or daily profiles.
- Full time series of hourly values of both solar radiation and PV performance.
- Typical Meteorological Year data for nine climatic variables.
- Maps, by country or region, of solar resource and PV potential ready to print.
- PVMAPS software includes all the estimation models used in PVGIS.

Following these trends, this work aims at stimulating the use of GIS in the PV plants O&M by organizing a Relational Database (DB), capable of collecting any information related to the PV plant itself. This different method, with the addition of spatial information, could bring forward innovative predictive and preventive maintenance systems in the future. This study aims to evaluate the potential of a specifically designed GIS tool in the location of PV faults and the analysis of faults' effects on PV power plants working in real operating conditions.

2.2 Use of GIS in the Urban Management and Risk domain

GIS platforms are containers for spatial information which, when properly managed, lead to the creation of queryable data systems, up to the creation of cartographic products at different territorial scales (e.g geo-environmental maps) and for different purposes (e.g. thematic maps). The literature presents a plethora of works exploiting GIS for several domains, including private/public gardens [32], spatial analysis [33], decision making [5], photovoltaic plants [34].

In other words, GIS allows visualising, combining and managing heterogeneous data from different acquisition techniques sensor network sources, insomuch warranting data sharing and interoperability [35]. Nowadays, emergency management plans or conservation actions at building level are entrusted on 3D data, high resolution photogrammetric images, cadastral data, urban planning data, building mapping (just to mention some), hitherto performed largely manually. Example of this interoperability, within the field of heritage conservation, could be found in the work carried out by Sánchez-Aparicio et al. [36] on which it is developed a GIS platform able to integrate 3D point clouds, 360º images, inspection forms and a wireless sensor network to manage the preventive conservation of heritage places.

At urban level, the management of emergency plans could be considered as a priority since they provide the necessary information for the designing of prevention and mitigation actions. In the field of urban safety, seismic, fire and flood risks, which can cause serious consequences, must inevitably be taken into account in order to plan prevention actions and adopt protection measures for the population [37]. The integration of risk plans into a GIS platform represents an efficient and effective solution towards risk mitigation at the urban scale, allowing administrative authorities to define interventions for a more accurate and comprehensive emergency planning strategies. Ortiz et al. in their studies on the historical center of Seville (Spain) use a GIS framework for designing risk maps through the spatial analysis of hazards (structural, environmental, anthropogenic), vulnerability maps and test of characterization [38, 39]. The integration of all this information allows to create a suitable strategy for prioritize preservation efforts. In the same line, Saha et al. uses the GIS platform for generating a multi-hazard susceptibility mapping for evaluating a cultural heritage site in the Himalayan region (India) [40].

With regard to seismic risk, many applications of data management through a GIS platform can be found in the literature, motivated by its versatility, and especially due to the open-source way of sharing information (e.g. QGIS, WebGIS). The evaluation of seismic vulnerability, urban resilience, and recovery strategies has been largely performed with GIS, in order to obtain the typological characterization of the surveyed buildings. As an example, in [41] authors proposed a methodology to create the seismic map identifying the building assessments and vulnerability. Moreover, a seismic risk evaluation method in a district level is proposed by [42]. The model assesses the seismic vulnerability using GIS for the definition of a vulnerability map. Furthermore, a geographical information system to study the seismic vulnerability of Tehran to an earthquake by taking in account different categories of information is proposed by [43] and a GIS-oriented procedure using geological and geotechnical parameters and also the vulnerability of buildings and the effects of their collapsing,

is suggested by [44]. Interested reader can find similar experiments in [45], where the authors defined a cross-mapping about vulnerability, damage scenarios and buildings exposure based on a multi-level procedure for earthquake disaster prevention. The same approach was adopted by Salazar and Ferreira which confirmed the multiple components of seismic risk to be managed within the GIS tool [46].

GIS platform is also suitable and useful for planning safety interventions and optimal routes for the accessibility of a certain area; the main novelty in this case was the assignment of priorities [47]. In the specific case of seismic analysis of buildings, there are several studies that address the issue of seismic vulnerability on a number of parameters describing individual building properties [48, 49]. These studies are typically addressed by the structural engineering sector that perform specific analyses of building stability. The results obtained from these analyses are useful for mapping the seismic assessment of buildings in an urban settlement and only in few cases GIS tools are used to draw thematic maps [50]. It is worth to mention the works carried out by Indirli et al. in which they propose the use of a GIS approach supported by the laser scanning technology and in-field works (AeDES, Agibilità e Danno nell'Emergenza Sismica, first level damage detection, emergency intervention and usability assessment form for ordinary buildings in post-seismic emergencies) as a quick survey tool for pre/post-earthquake building inventories in the Italian region of Abruzzo [51, 52]. In comparison with these previous works, the work in this thesis aims at improving at different levels:

1. the integration of additional geomatic techniques such as the use of structure from motion approach for the creation of high-resolution 3D point clouds of the roofs or the use of 360º images from the lidar scans to support the virtual inspection of the surveyed object in a GIS;

2. the automatic extraction of geometrical parameters and attributes required for the seismic risk assessment;

3. the use of GIS mobile app to support the in-situ data acquisition.

Chapter 3

Methodology and case studies

In this chapter, the methodologies studied for each domain will be explained and case studies on which they have been tested will be introduced.

3.1 PV plants Thermographic Inspections and Management in GIS

PV plant O&M follows a well-defined pipeline, in which a relational database plays a key role (Figure 3.1).

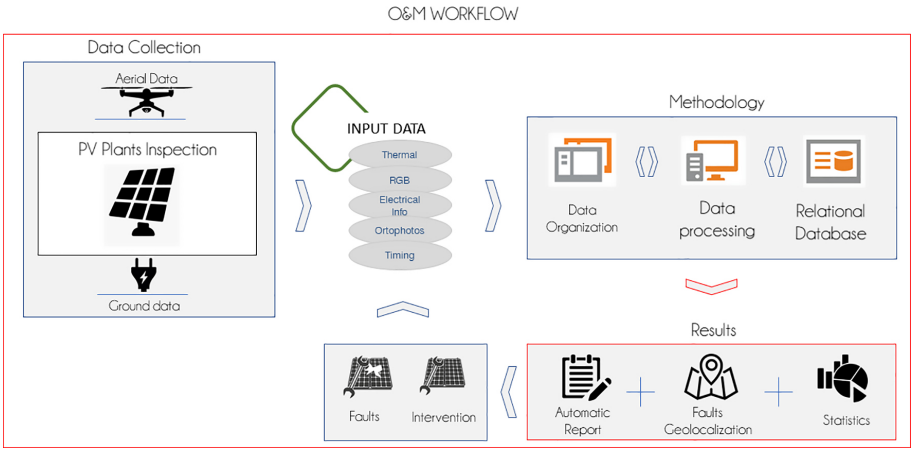

Figure 3.1: Workflow adopted for the O&M in PV plants.

This workflow starts with the data acquisition from aerial and ground sources; such data are the input managed within the GIS solution, following the relational conceptual model. As a result, the user can extract all the information for a more efficient O&M. O&M is seamless, as data can be constantly updated.

The creation of a relational database requires a tidy process of data organization, making any information linked to each other with a relational structure. In the case of PV plants, information is both qualitative and quantitative.

To build a database model with a good data connection and organization, and, finally, to test its functionality, data from two PV plants in Italy were used. The first was installed on the roof of an industrial shed in the province of Cuneo (Plant A) and the second was located in a countryside in the province of Pescara (Plant B).

These data have been kindly provided by Solis s.p.a. and Flyengineering s.r.l. in anonymous form in respect of the privacy of the owners of the plants.

3.1.1 Data Collection and Processing

In this section the main data about PV plants and how they are usually collected will be illustrated.

Orthophoto of the PV plant through Aerial Photogrammetry

A very important piece of information is the orthophoto of the PV system, since it constitutes the reference on which to digitise all the elements of the plant that will be included in the geodatabase. For its creation, it is nowadays usually convenient to use an UAV to capture aerial photos to be processed using the photogrammetric technique.

In these two case studies, for the execution of the survey an *"SR-SF6"* has been used. It is a VTOL UAV, produced by Skyrobotic s.p.a., which has a total width of 1.2 m and a weight of 2 kg without payload. It can lift off a maximum total weight of 4.8 kg, and can fly in winds up to 12 m/s with gusts of 16 m/s. This UAV can fly both in manual and in automatic mode, following a flight plan designed and assigned via tablet, using Skyrobotic's proprietary app, SkyDirector (Figure 3.2) [53].

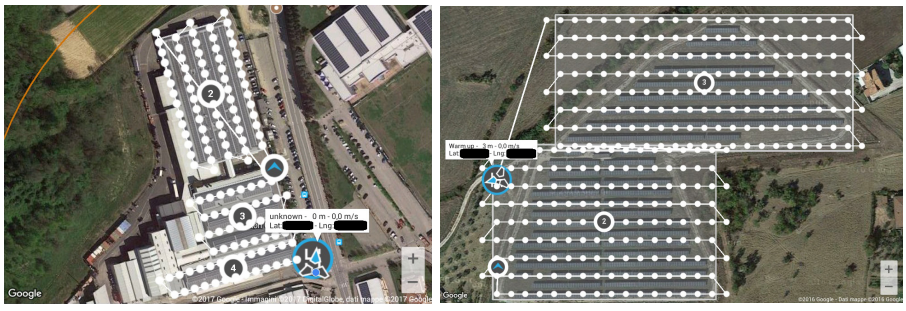

(a) (b)

Figure 3.2: The flight plans designed using the SkyDirector app, for the aerial data acquisition. (**a**) and (**b**) depict the flight plans used for Plant A and Plant B, respectively.

In both cases, the flight was set at a 50 m height from the ground, 40 m from

the survey object, with 70% overlap and 60% side lap. The flight plan was then generated by the SkyDirector app according to the optics of the selected payload, a Sony DSC-QX100 [54], a digital camera with a resolution of 20 Mpx.

The photos acquired during the aerial photogrammetric survey were processed by using a Structure from Motion approach [55]. This approach allows us to obtain a 3D point cloud model and an orthophoto of the surveyed area. The inner orientation of the camera was carried out by using a self-calibration approach, considering a Fraser camera model [56]. The external orientation of the cameras was performed by using the self-calibration approach as well as a bundle adjustment.

If the survey must be georeferenced, it is possible to acquire the coordinates of some points (3 minimum) to be used as *Ground Control Points* (GCP) in the bundle adjustment phase. However, even when it is not the case, at least the distance between two points on the object must still be acquired to enable the reconstructed object to be scaled correctly.

Then, a Semiglobal Matching stage was performed with the aim of obtaining the dense point cloud [57].

The point cloud obtained is then used to reconstruct a mesh of the survey object. In case a textured 3D mesh of the survey object is needed, a UV map can be calculated and the texture coloured by projecting on the mesh the most appropriate images for each area.

The production of the *orthophoto* (Figure 3.3) follows a very similar procedure, but only the parts visible from its direction need to be coloured. In fact, each pixel of the orthophoto is projected onto the mesh to calculate the three-dimensional position of the point in the reconstructed model, and is then coloured according to the images from which that point is visible.

So as already mentioned, if a plant plan in vectorial format is not available, the various components of the PV system can be digitised by tracing the orthophoto. This can be done directly in a GIS or it is possible to use the advanced drawing tools of a CAD, which are convenient for regular and repetitive objects such as PV grids, and then re-import the digitised vector objects into the GIS.

Electrical information of the PV plant

Other data concerning PV systems are acquired from the ground in more traditional ways. This is the case, for example, with the *I–V curve* (current–voltage characteristic curve) tests, which are performed on individual modules or on the modules connected in series in a string. Using a special instrument called an I–V curve tester, current–voltage characteristics are measured under the operating conditions of temperature and irradiance, and corrected to standard

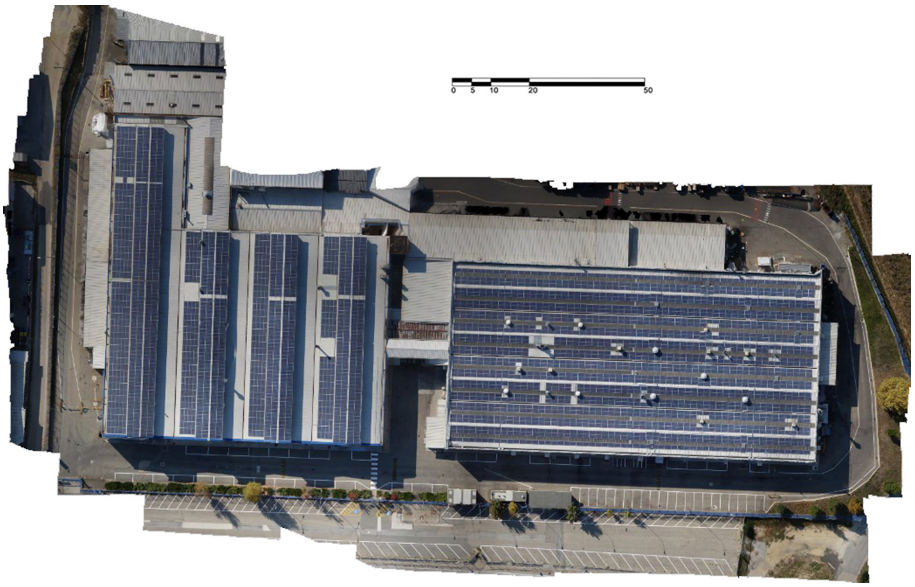

Figure 3.3: Orthophoto of the PV plant (Plant A).

test conditions. Afterwards, the final check consists of verifying if the supplied power falls within the tolerance declared by the manufacturer [58].

Another check that is carried out on photovoltaic systems is to calculate the *performance ratio* in terms of power. This key performance indicator highlights the overall effect of losses on the power generated in alternating current. These losses are due to the incomplete exploitation of solar radiation, the conversion efficiency of the inverter and component failures or inefficiencies [59].

In order to test the database functionalities, the monthly and annual energy production data—which were not in our possession—have been assumed. These are usually measured for the entire plant and for individual inverters.

Aerial and ground thermal inspections

The life span of a photovoltaic system is dependent on that of its components. While the modules in the worst case give good performance for about 20 years with a common 0.5% annual degradation, unless they have critical issues, the lifetime of the inverters can vary widely depending on the climate of the installation site [8, 60].

The major cause of damage to the inverters is the too-high temperature to which they are subjected in the absence of a good cooling system. For the modules, the main factors of performance loss are instead: light induced degradation, solder fatigue failure, silver grid finger delamination, bypass diode failure, delamination, cell cracks, corrosion, polymeric discoloration, ultraviolet

degradation of the cell, polymeric mechanical failure, and potential induced degradation [61].

The aerial thermal inspections operations are usually performed by capturing infrared and visible images of the plants from drones in order to find and locate the overheated components compared to others of the same type. Overheating means that the component is broken or at least not working properly [62, 63]. This information is fundamental to be included in a management system, to provide the producer with an agile tool to manage O&M procedure.

It is recommended, for a good thermal inspection, to avoid the time periods in which parts of the system are shadowed. The best timeframe is usually at noon, when the PV plant is at the maximum power production conditions, if the sky is clear.

For the first case study (Plant A), aerial thermal images have been collected with the same drone mentioned above, using a Flir Tau 2 640 thermal camera, with a resolution of 640 × 512 pixels and a focal length of 13 mm [64]. Instead, for the second case study (Plant B), a Flir E75 [65] has been used from the ground to inspect individual modules that have shown abnormal overheating, or switchboards and inverters, more closely.

Figures 3.4 and 3.5 show data acquired from aerial and terrestrial thermal inspections respectively, with visible examples of overheated components.

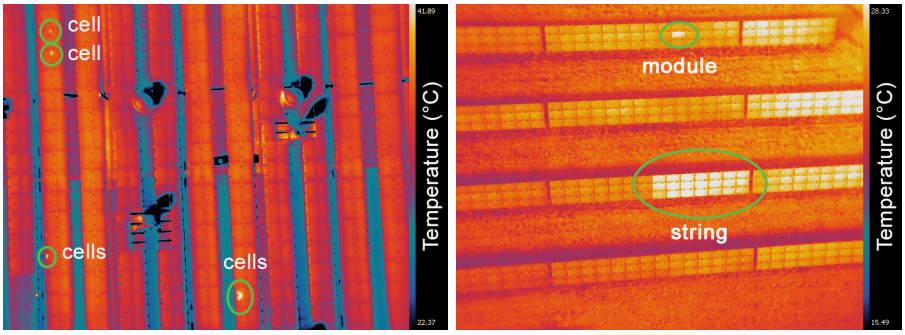

(a) (b)

Figure 3.4: Thermal images collected from UAV. (**a**) Example of overheated cells, also called a hotspot, (Plant A), and (**b**) an example of an overheated module and string (Plant B).

Overheated components detection and classic report production

Depending on the type of camera and the format of the files produced, there are specific programmes that allows to customise the visualisation mode and export the files in other formats. For example, it is possible to set up *false colours* by

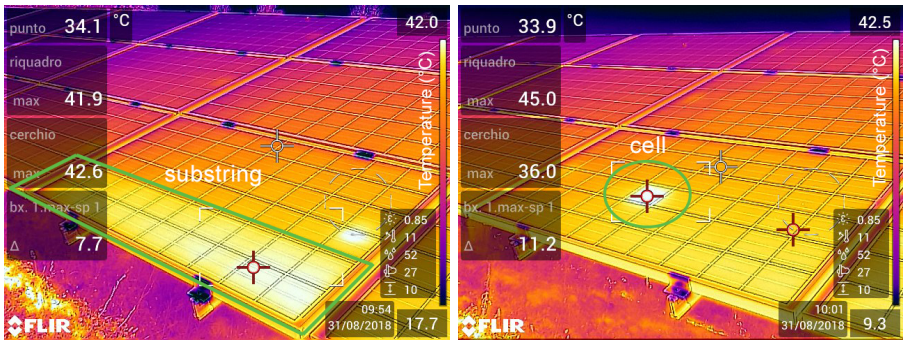

(a) (b)

Figure 3.5: Thermal images collected from ground level showing overheated elements (Plant B). (**a**) is an example of overheated substring probably due to a bypass diode fault, and (**b**) is an example of overheated cell, also called a hotspot.

choosing between different colour scales and configuring the *temperature range* to be shown.

Nevertheless, following *common workflows* takes an enormous amount of time and effort for the report production. In fact, in order to redact a classic inspection report, an expert technician must analyze the thermal images in sequence to identify the overheated components, using the flight plan as a help to understand which part of the plant is shown.

Every overheated module, string and field must be noted on a map (Figure 3.6) and listed on a table, with an identification system and the indication of the thermal images in which they are visible.

Automatic Faults Detection with Deep Learning Algorithm

A significant help in speeding up the production of these reports is the adoption of deep learning algorithms that can automatically identify the overheated components (anomalies) in thermal images from UAVs.

Therefore we have partnered with the Vision, Robotics and Artificial Intelligence (VRAI) research group of the Department of Information Engineering (DII), at Università Politecnica delle Marche, for the development of solAIr, an artificial intelligence system based on deep learning for the detection of overheated components in aerial thermal images of PV plants [66]. This system is based on the mask region-based convolutional neural network (Mask R-CNN) architecture, adopted because it simultaneously performs object detection and instance segmentation, making it useful for the automated inspection task. The proposed system is trained and evaluated on the photovoltaic thermal images dataset, a publicly available dataset collected for this work. Furthermore,

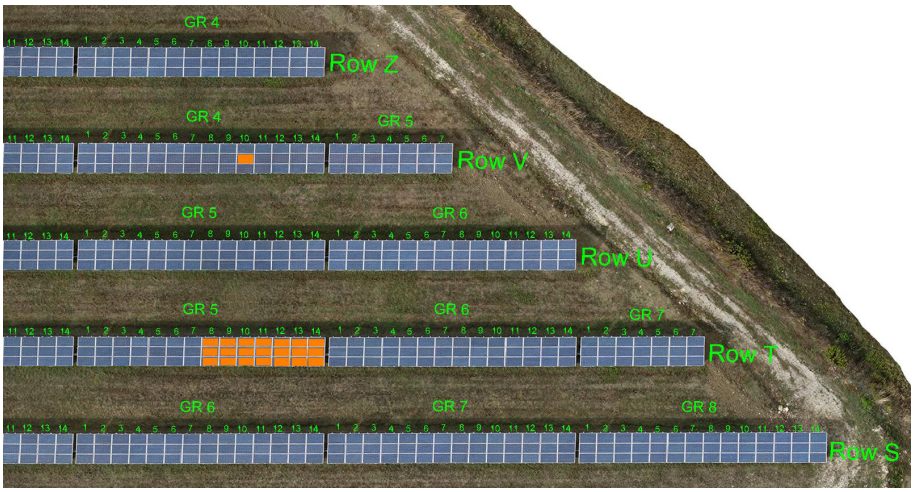

Figure 3.6: Example of a manually produced map report about a PV thermal inspection.

the performances of three state-of-art deep neural networks, (DNNs) including U-Net, FPNet and LinkNet, are compared and evaluated.

To train and evaluate this system, we provided a new dataset consisting of aerial thermal images from inspections carried out by Flyengineering on large-scale PV plants in South Africa, to have a great number of images, and we have made it available to download for research purposes [1] [66].

In this dataset the images may present one or more anomalies, as depicted in Figure 3.7, and has associated a single mask that segments each anomalous cell. In case of a portion of contiguous anomalous cells, the operator segments the whole portion in a single block. The pre-processing and annotation phase produced a dataset of 1 009 thermal images, including each respective mask. The thermal images and the binary masks have the same dimensions of 512×640 pixels.

The input classes were chosen according the following three types of annotation:

- Images with one anomalous cell (Figure 3.7a,b);
- Images with more than one anomalous cell (Figure 3.7c,d);
- Images with a contiguous series of anomalous cells (Figure 3.7e,f).

The number of images per class are reported in Table 3.1.

[1] PV thermal images dataset download link: `http://vrai.dii.univpm.it/content/photovoltaic-thermal-images-dataset`

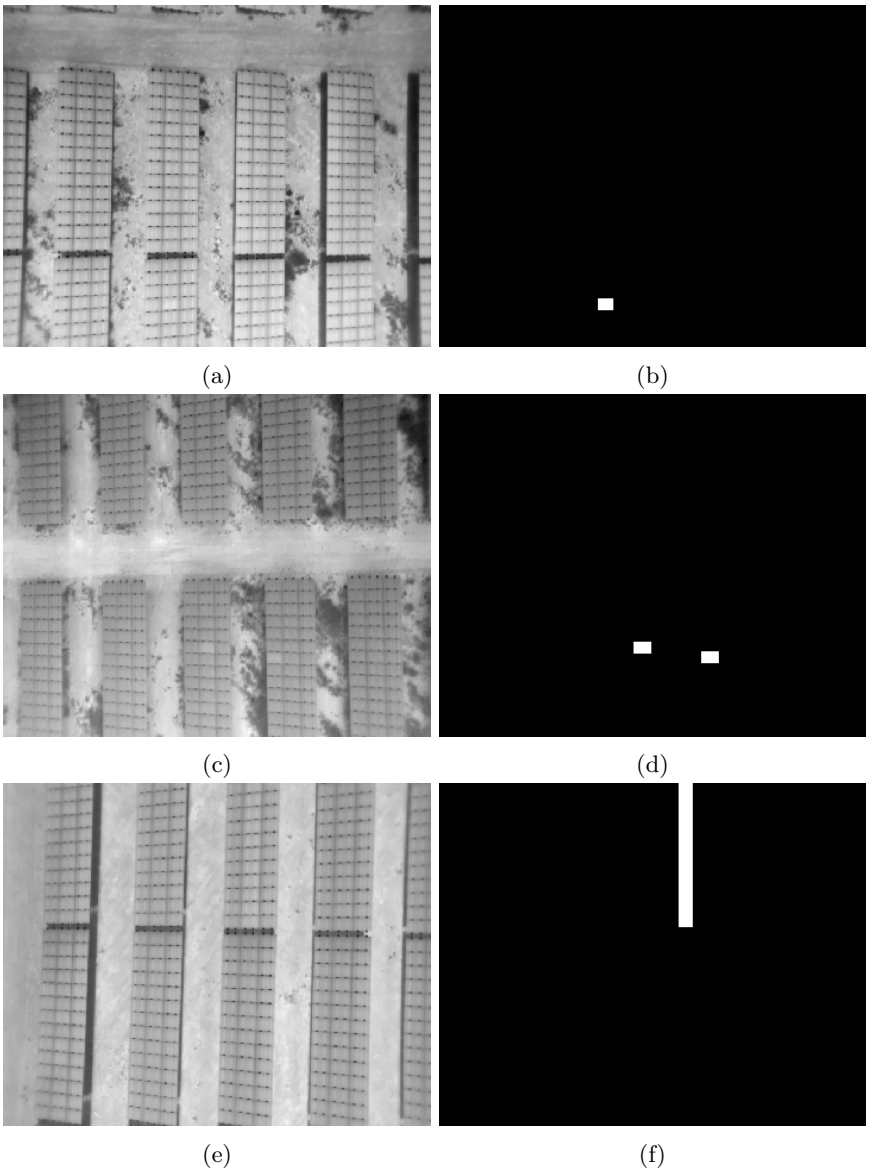

Figure 3.7: Examples of images from the dataset. Figures (**a**,**c**,**e**) are normalized thermal images. Figures (**a**,**c**,**e**) depict examples of masks, where the black color is the background that contains all the cells without anomalies and the white is the cells with anomalies. Figure (**b**) is an example of mask with a single anomaly cell; Figure (**d**) is a mask with two separated cells with anomalies; Figure (**f**) is a mask with continuous cells that present an anomaly.

Table 3.1: Anomalies statistics.

Class	**Images**
One Anomaly	841
Not Contiguous Cells with Anomalies	116
Contiguous Cells with Anomalies	52
Total Dataset	**1009**

Image segmentation techniques take as input an image and output a mask with the predicted anomalous cells. Since it is a binary segmentation, the mask has pixels with values equal to 0 for the background and 1 for the anomalous cell. The DNNs specifically designed for image segmentation use convolutional neural networks (CNNs) for image classification as backbones for feature extraction, and on these backbones different kinds of feature combinations are constructed to achieve the segmentation result. CNNs are the most successful, well-known and widely used architectures in the deep learning domain, especially for computer vision tasks. They are a particular neural network that is able to extract discriminant features from data with convolution operations, so they can also be used as feature extraction networks. In this work, the backbone of the three segmentation networks is based on EfficientNet [67]. Based on the backbone extracted features, the three segmentation methods that are compared for the development of our system are: U-Net [68], LinkNet [69] and feature pyramid network (FPN) [70]. All these techniques give as output a single overall mask containing all the anomalous cells predicted in the same input image.

Instance segmentation instead requires a mask to be created for each anomalous cell within the same image. It has been chosen for this work mainly because it directly provides the correct position of the anomalous cell, an advantage for the operator, while image segmentation needs a further step to split all the defective cells calculated within the overall mask mentioned above. Following this assumption, Mask R-CNN was proven to be an effective and accurate network for solving these problems [71]. It is based on Faster R-CNN [72] and has an additional branch for predicting segmentation masks on each Region of Interest (RoI) in a pixel-to-pixel manner. Considering the specific case of anomaly cells detection, this network is not trained directly with image masks, but it needs the anomalous cell bounding boxes within the image: not a single mask, but a set of top-left and bottom-right coordinates of each bounding box. Furthermore, in order to be compared with image segmentation techniques, it also needs a post-processing step: all the anomalous predicted cells have to be merged into one overall mask.

3.1.2 Database Organization and Data Relations

In this section, the *conceptual model* developed will be illustrated. It follows a data structure proposed where all data can be stored and analysed for the management of PV plants, allowing us to *query* and to generate *automatic reports*, overcoming the limitation of the common workflows.

The creation of a management system to be exploited in a GIS involves the creation of a *Geodatabase* where any information is related to a map; the consequent GIS model allows the managers of the PV plants to identify power losses caused by affected PV modules and to keep track of the overall performance of the power plant. The database implementation correlates the tables containing all the categories of data, which will be described below, with one-to-many connections in order to cross-reference these data and perform various types of analysis. Many of these tables contain *georeferenced* geometric vector data, which can be used to perform *spatial analyses*. In addition, GIS allows you to import geo-referenced raster data as satellite images or orthophotos.

To improve the readability and understanding of the database model, several tables have been grouped according to the different topics of the data stored.

PV plants and main components group

Depending on the type of PV system, some specific components may be present or not, so a brief description of the main ones that are always present is worthwhile and is given in hierarchical order below.

- *Cells* are the fundamental elements of the modules; the main function is to convert the energy of solar radiation into electrical energy, in the form of direct electric current.
- *Substrings* are formed by cells electrically connected in series, in such a number as to reach the designed output voltage from the module.
- *Modules* are the basic products which compose a PV system. They consist of identical substrings electrically connected in parallel, in such numbers as to obtain the designed current intensity and nominal power at the output of the module.
- *Strings* are in turn formed by modules electrically connected in series in a number, chosen by the system designer, to reach the optimal inverters' working voltage, without exceeding the maximum allowed.
- *Arrays* are composed of strings, connected in parallel and chosen by the system designer, so as not to exceed the maximum current intensity and power allowed in the inverter input.

- *Switchboards* are the electrical panels at the main junctions where all the wiring connecting the arrays to the inverters passes through.
- The *inverters* convert the direct current coming from the photovoltaic arrays into alternating current, allowing its use or distribution. They also have control functions.

This glossary, which does not have the ambition to cover all the terminology related to the PV sector, follows the nomenclature reported in the current European legislation [73].

This hierarchy will also be maintained in the relational structure of the developed information system, especially in the group of tables about the plants and their main components (Figure 3.8). It contains the tables corresponding to the *components* described above, apart from cells and substrings, together with the tables *"status"*, *"owners"*, *"plants"*.

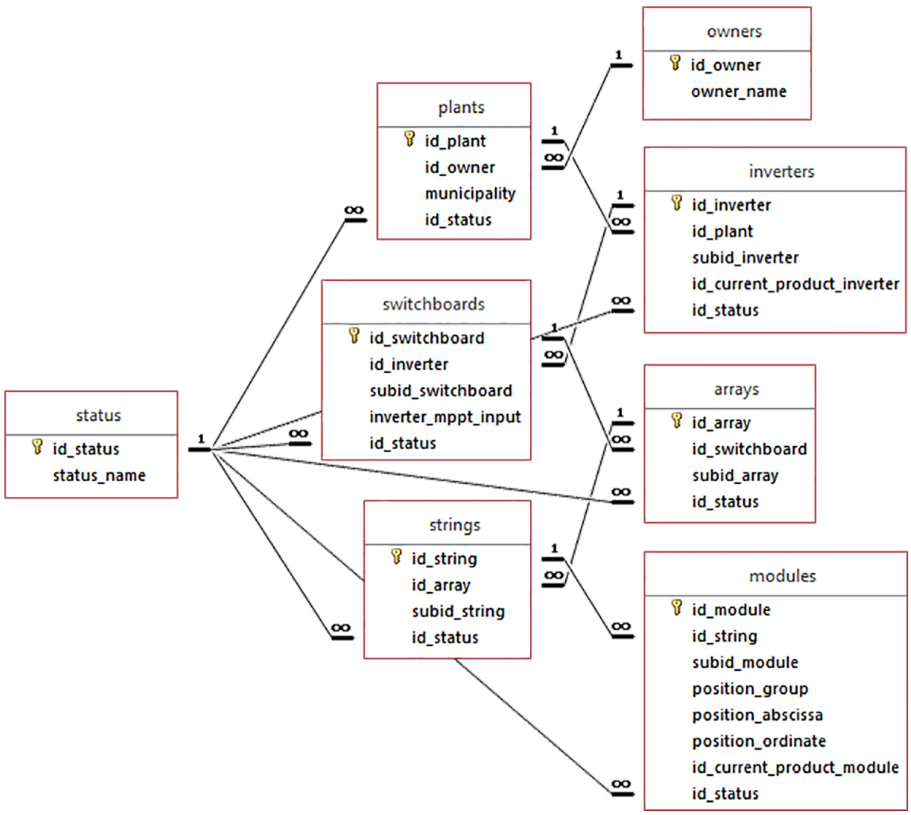

Figure 3.8: The main group of the conceptual model implemented into the relational database.

Every record in these tables has its own unique ID and the ID of the superior

element in the hierarchy, which it is linked to. The unique IDs are formed by the union of the superior element's ID and the sub IDs (different for each component belonging to the same superior element) separated by a dash. In these tables and in the plants table, the *"id_status"* field links the records with the *"status"* table, in order to indicate the status of the element.

The *"status"* table contains all the possible statuses of the plants and their components, defined by the fields *"id_status"* and *"status_name"*. For example, these statuses could be *"on"* or *"off"*, but others can also be added if necessary.

The *"owners"* table can be useful for plant management companies, in fact it could contain all the data about the various owners who can be linked to their plants inserting their IDs in the plants table.

The *"plants"* table also contains the *"municipality"* field to specify the administrative zone where the plant is located.

The *"inverters"* and *"modules"* tables include the *"id_current_product_inverter"* and the *"id_current_product_module"* fields, to indicate which commercial products of the *"products_inverters"* and *"products_modules"* tables are currently installed.

The *"modules"* table also includes the *"position_group"*, *"position_abscissa"* and *"position_ordinate"* fields in order to locate the modules using a custom reference method based on the counting of the modules in the various groups.

Products group

The group of tables about the products consists of the *"manufacturers"*, *"products_inverters"*, *"products_modules"*, *"products_thermal_cameras"*, *"products_iv_curve_testers"* and *"products_performance_ratio_measuring_devices"* tables (Figure 3.9). It is useful to keep track of the commercial products that have been used to build the plants and to perform tests and inspections.

In the *"manufacturers"* table each record represents a company that produces components for PV construction, such as inverters or modules, or instruments used to perform tests or inspections on PV plants. It may be expanded with all company references, but, in this example, only the *"manufacturer_id"* and *"manufacturer_name"* fields are present.

All the product tables contain the commercial products identified by their IDs, formed by the union of the *"id_manufacturer"* and their subID (different for each product of the same manufacturer). They also include the fields *"product_number"* and *"product_name"*.

The *"products_inverters"* and *"products_modules"* tables also contain the main technical specifications.

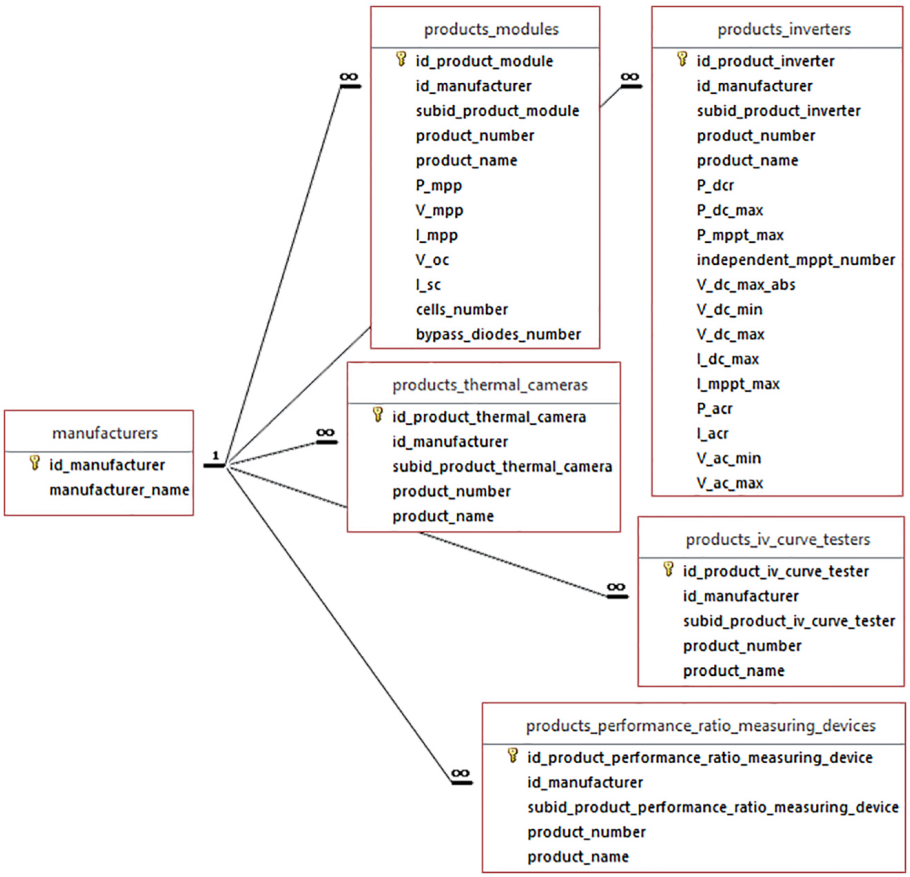

Figure 3.9: The products group of the conceptual model implemented into the relational database.

Operations group

The group about the operations is useful to keep track of all the operations performed on the PV plants and their components. It includes the *"executors"*, *"operations_categories"*, *"operations"*, *"operations_inverters"*, *"operations_switchboards"*, *"operations_arrays"*, *"operations_strings"* and *"operations_modules"* (Figure 3.10).

The *"executors"* table is also part of the *"aerial thermal inspections"*, *"terrestrial thermal inspections"*, *"I-V curve tests"* and *"performance ratio checks"* groups; in fact, each record represents a company executing operations, inspections, tests or checks. It may be expanded with all company references but, in this example, are only present the *"id_executor"* and *"executor_name"* fields.

The table *"operations_categories"* is useful to indicate the various types of operation performed on the plants. It includes the fields *"id_operation_*-

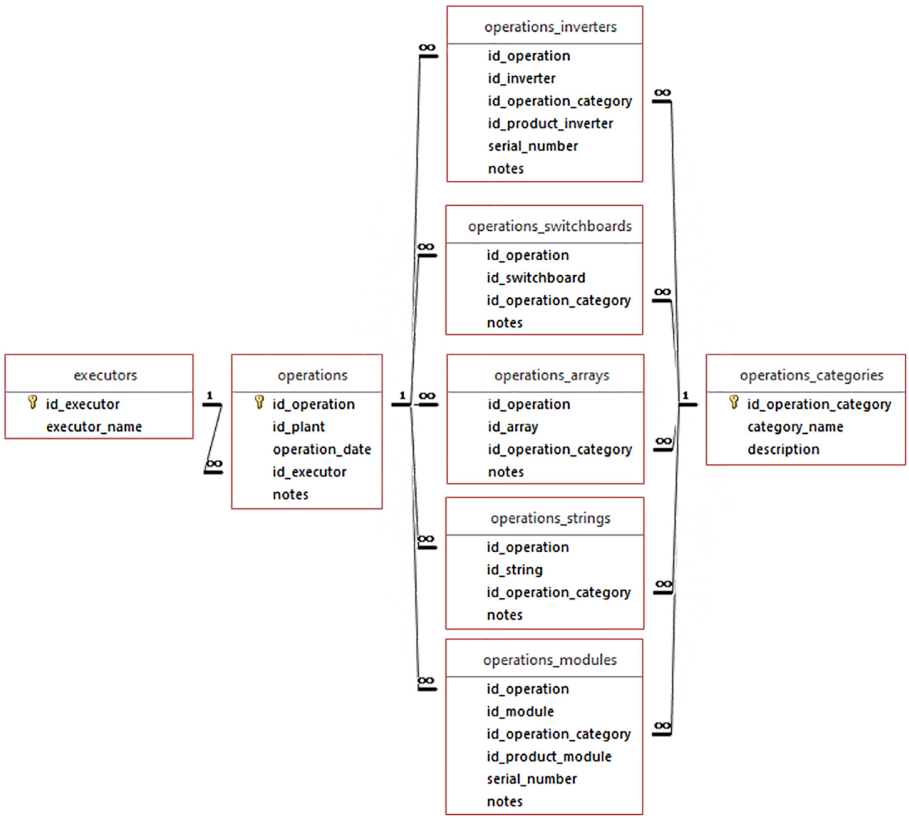

Figure 3.10: The operations group of the conceptual model implemented into the relational database.

category", *"category_name"* and *"description"*.

Every operation performed by an executing company on a PV plant is stored in the *"operations"* table and is defined by the fields *"id_operation"*, *"id_plant"*, *"operation_date"*, id_executor" and *"notes"* (to annotate specific aspects about the operations).

Each record stored in the tables *"operations_inverters"*, *"operations_fields"*, *"operations_strings"* and *"operations_modules"* indicates on which components each operation had been performed. These tables include the fields *"id_operation"*, the id of the specific component, *"id_operation_category"* and *"notes"* (to annotate specific aspects about single components in an operation).

The *"operations_inverters"* and *"operations_modules"* tables also include the *"id_product_inverter"* and *"id_product_module"*, other than the *"serial_number"*, field to identify it uniquely.

Aerial thermal inspections group

The group about the aerial thermal inspections includes all the tables needed to store all the data from the aerial thermal inspections, such as *"executors"*, *"weather_conditions"*, *"aerial_thermal_inspections"*, *"aerial_thermal_photos"*, *"aerial_thermal_inspections_arrays"*, *"aerial_thermal_photos_inspections_arrays"*, *"arrays_defect_types"*, *"aerial_thermal_inspections_strings"*, *"aerial_thermal_photos_inspections_strings"*, *"strings_defect_types"*, *"aerial_thermal_inspections_modules"*, *"aerial_thermal_photos_inspections_modules"* and *"modules_defect_types"* (Figure 3.11).

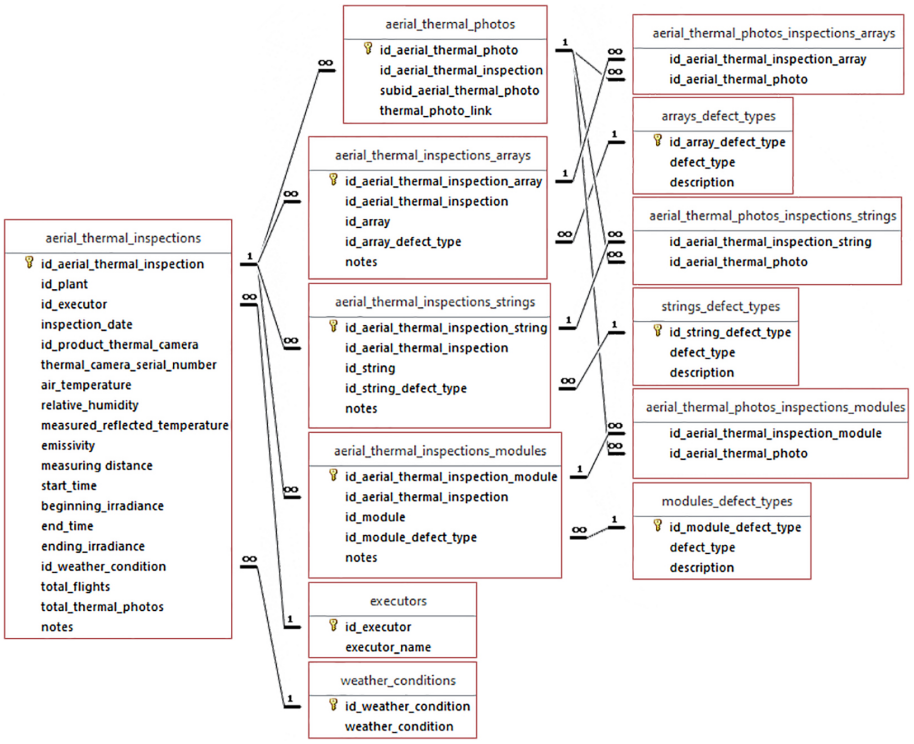

Figure 3.11: The aerial thermal inspections group of the conceptual model of the relational database.

The *"executors"* table is the same described above.

The *"weather_conditions"* table contains the standard definitions for weather conditions and is also part of the *"terrestrial thermal inspections"*, *"I-V curve tests"* and *"performance ratio checks"* groups.

The *"aerial_thermal_inspections"* table provides general information about the inspection campaigns, such as the plant on which they are performed, the executor, the inspection date, the thermal camera that was used, the environmental conditions and any notes.

All the links to the thermal photos are stored in the *"aerial_thermal_photos"* table, defined by the fields *"id_aerial_thermal_photos"*, *"id_aerial_thermal_inspection"*, *"subid_aerial_thermal_photo"* and *"thermal_photo_link"*.

Each record in the *"aerial_thermal_inspections_arrays"*, *"thermal_inspections_strings"* and *"thermal_inspections_modules"* tables indicates if the relative component is totally, partially, or not overheated during an aerial thermal inspection campaign, thanks to the connection to the defect types table of the relative component. They also include the id field (formed by the union of the *"id_aerial_thermal_inspection"* and the id of the relative component, also present in the tables) and *"notes"* (to annotate specific aspects about single components in an inspection).

The *"aerial_thermal_photos_inspections_arrays"*, *"aerial_thermal_photos_inspections_strings"* and *"aerial_thermal_photos_inspections_modules"* tables permit to link the results of the single components inspections with the multiple corresponding aerial thermal photos in which they are visible. Each record in these tables contains the two ids of the records to connect from the two tables.

Terrestrial thermal inspections group

The terrestrial thermal inspections group is similar to the one just described regarding aerial thermal inspections, with the difference that terrestrial thermal inspections are performed on individual modules, switchboards or inverters (Figure 3.12).

In contrast to aerial thermal inspections, thermal photographs of different sub-elements of the same component are acquired in terrestrial inspections.

In particular, in the tables that connect the inspections on the components with the multiple thermal photos of the various sub-elements, the measurements of the maximum temperature of the sub-element, the reference temperature and the temperature difference are stored. In addition, the connection with the defect type tables is also provided so that it can be specified for each photo of each sub-element.

In the *"terrestrial_thermal_inspections_switchboards"* table there is also the field *"measured_DC"* used to specify the direct current intensity measured in the switchboard during the inspection.

IV curve tests group

The group of the I–V curve tests includes all the tables necessary to contain the data of these tests that can be performed on strings or individual modules (Figure 3.13).

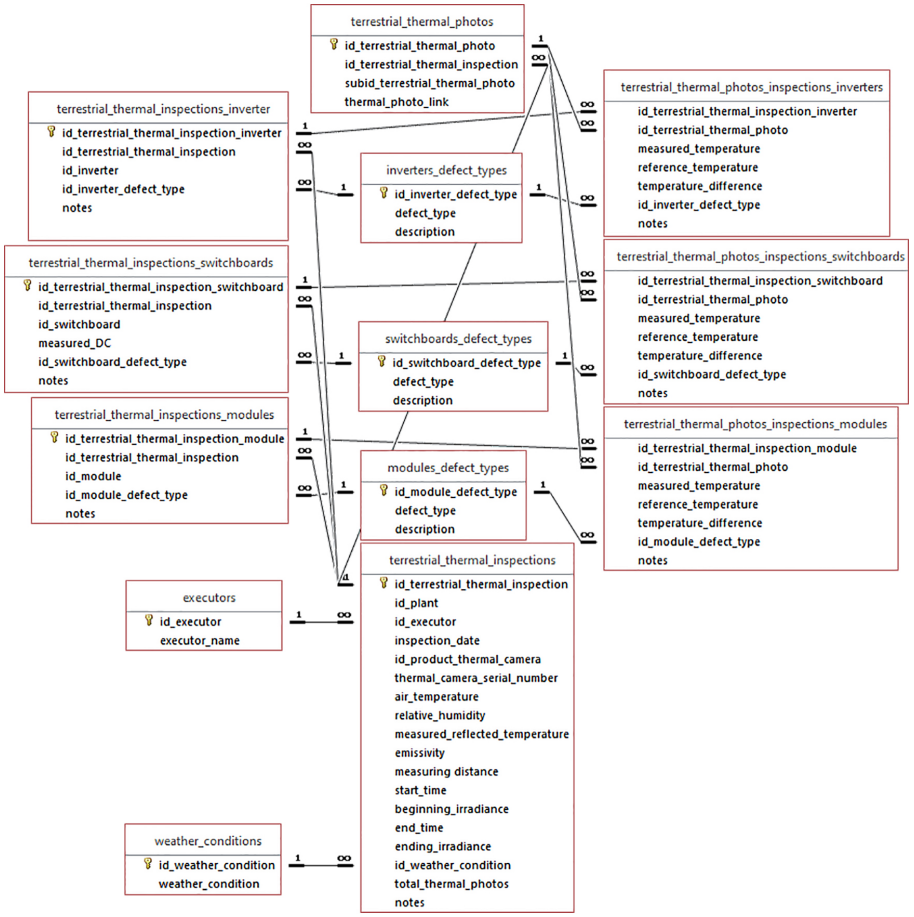

Figure 3.12: The terrestrial thermal inspections group of the relational database.

The *"executors"* and *"weather_conditions"* tables are the same described above.

The table *"iv_curve_testing_campaign"* provides general information about the testing campaign, such as the plant on which it is performed, the executor, the date, the I–V curve tester used and any notes.

In the *"iv_curve_strings_tests"* and *"iv_curve_modules_tests"* tables are stored all the electrical measurements performed with the I–V curve tester, in compliance with the regulations [58]. These tables also provide the connection to the *"iv_curve_tests_results"* table containing the possible results of the I–V curve tests.

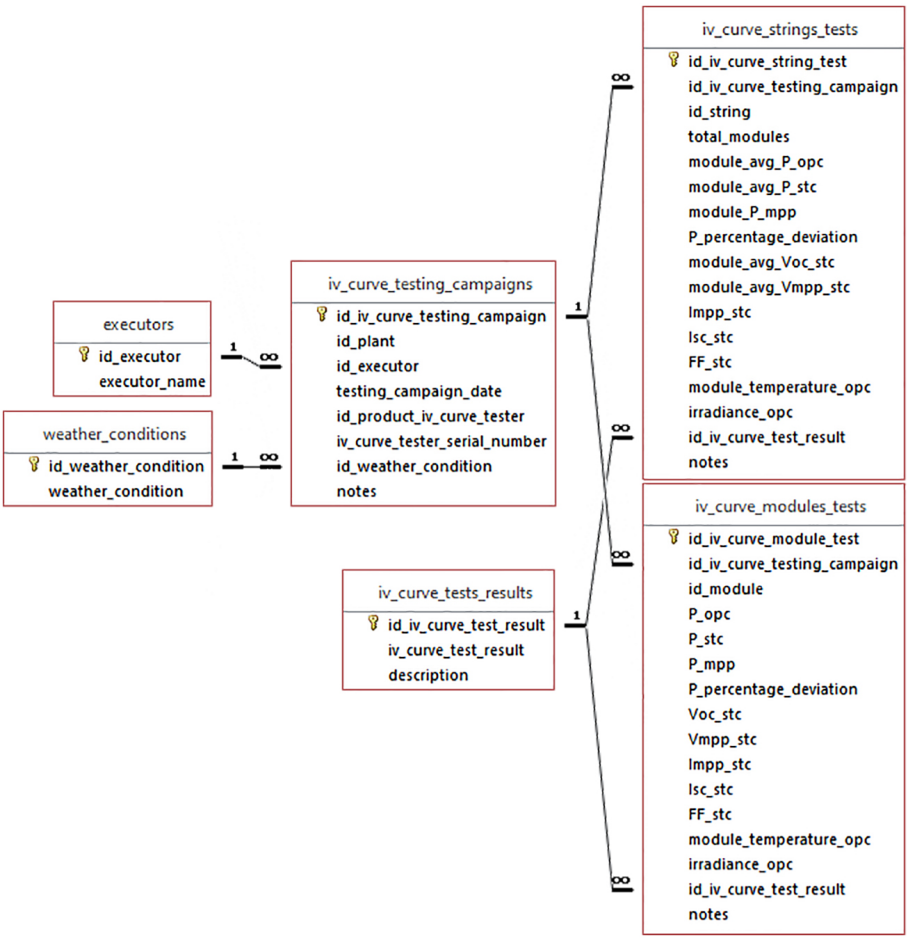

Figure 3.13: The IV curve tests group of the relational database.

Performance ratio checks group

The group of the performance ratio checks includes all the tables necessary to contain the data acquired during the checks performed on the inverters (Figure 3.14).

This group of tables is very similar to the one just described on the I–V curve tests. The only differences relate to the instrument, which is the performance ratio measuring device, and the electrical measurements performed—which are different, since they are in accordance with the regulations for the performance ratio tests [74].

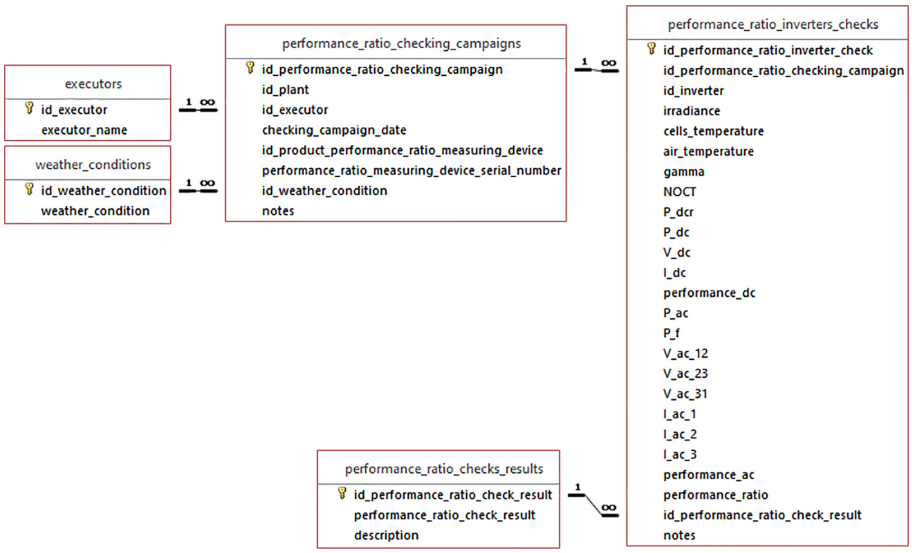

Figure 3.14: The performance ratio checks group of the relational database.

Energy production data group

The last group of tables is the one concerning energy production data (Figure 3.15).

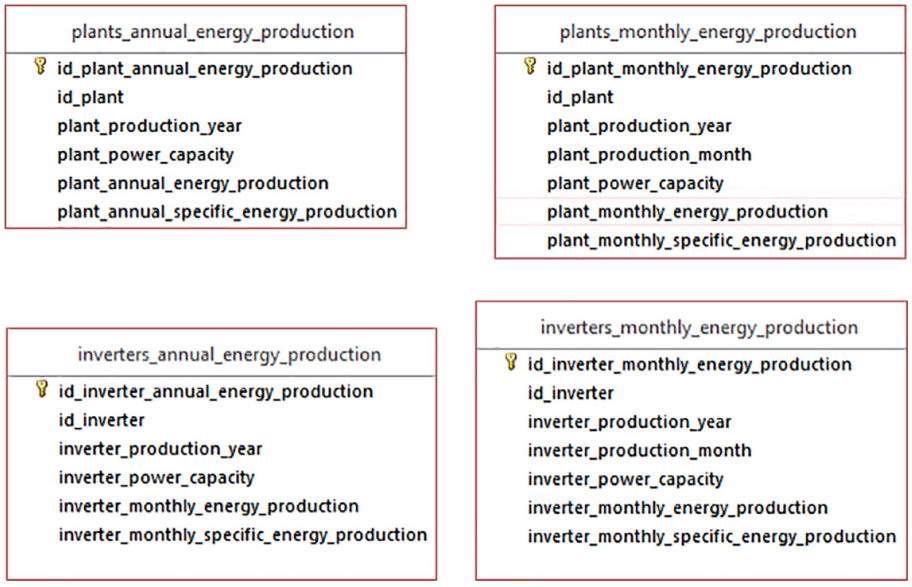

Figure 3.15: The energy production data group of the relational database.

The four tables in this group are able to store data on the energy produced

monthly and annually and measured for whole plants and individual inverters. In each table is stored the energy produced, the rated power capacity and the specific energy produced, obtained by dividing the energy produced by the rated power capacity.

3.2 Urban Surveys with Photogrammetry and TLS in GIS

Regarding the urban surveys, the aim of this work is to implement a GIS-based approach combining data from geomatic surveys and other non-metric data for the building assessment of a historical village after seismic events and to automatically extract information regarding geometric parameters of buildings, often used for a preliminary assessment of seismic vulnerability. In particular, point clouds are obtained from LIDAR (Light Detection and Ranging) and photogrammetric surveys from UAVs (Unmanned Aerial Vehicles). They are georeferenced using GCPs (Ground Control Points), obtained from GNSS (Global Navigation Satellite System) surveys, and combined. The laser scanner used is equipped with a digital camera which provides 360° images. As outputs of the data processing phase, the orthophoto is generated from the photogrammetric data, while DSM (Digital Surface Model), DTM (Digital Terrain Model) and building contours are extracted from the unified point cloud. Then, orthophotos, DSM, DTM, building contours, unified point cloud, 360° images and AeDES sheets are together collected and included in an open source GIS (QGIS). Finally, DSM, DTM and building contours are exploited to automate the extraction of information related to geometric parameters concerning the buildings, through Python scripts developed by the authors that interact with the data and objects in QGIS.

This methodological pipeline, described above, is summarized in Figure 3.16.

3.2.1 Case study

The seismic crater defined following the recent earthquakes that hit central Italy (2016, 2017) covers a very large area including 140 municipalities in four Italian regions, an area classified with a high seismic risk index (Figure 3.17). This area is characterized by a predominantly hilly and mountainous context of great landscape value and the urban realities present are mainly represented by small villages that are an example of tangible heritage for their historical, architectural and traditional-popular richness. To see these small towns lost and abandoned would be a great loss for the country, not only in terms of tourism, but also in cultural and economic terms.

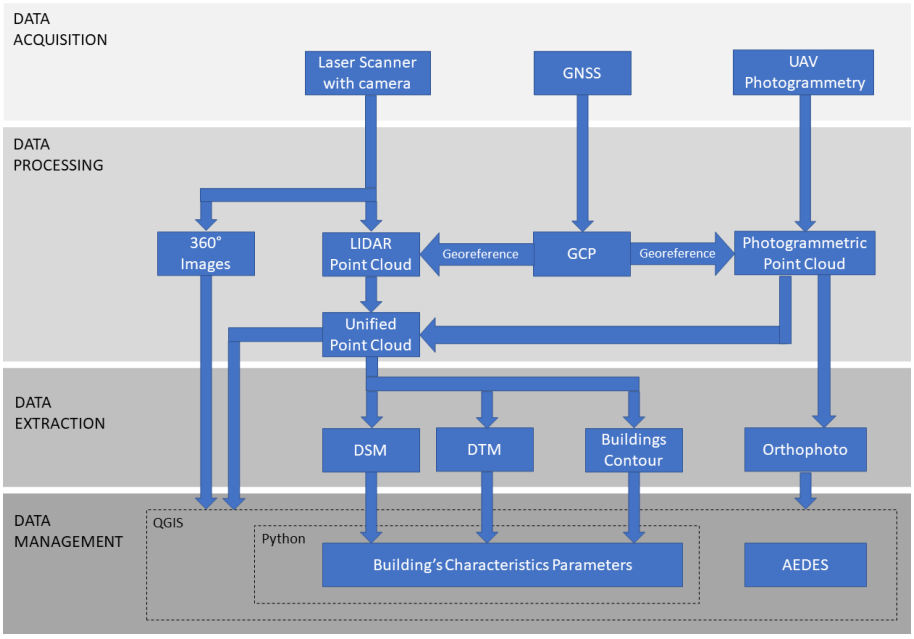

Figure 3.16: Methodology workflow.

The village Gabbiano (Pieve Torina), located within the earthquake crater in the Marche region (Figure 3.17), was identified as a case study for this research project on the implementation of a multi-data GIS system for building assessment. The village stands on a small hillside and consists in a small urban core, of about 21 building units in 12 clusters, of two-three storey buildings. These buildings are made up by two-three leaf irregular masonry covered by a timber structure with ceramic tiles.

After the seismic events the village has suffered significant damages on which part of the structures have collapsed, showing in-plane and out-of-plane mechanisms (Figure 3.18) and is still an area at risk and therefore uninhabited, being necessary the use of remote sensing strategies for generating the data required for the post-earthquake evaluation.

3.2.2 Technical documentation

In Italy, inspection campaigns made by the Civil Protection are carried out with the aid of the first level damage detection, emergency intervention and usability assessment form for ordinary buildings in post-seismic emergencies (AeDES) [75, 76]. The AeDES sheets were used for the first time by the Marche region in its original version during the 1997 Umbria-Marche earthquake. It was therefore used during the 2009 Abruzzo earthquake and subsequently in

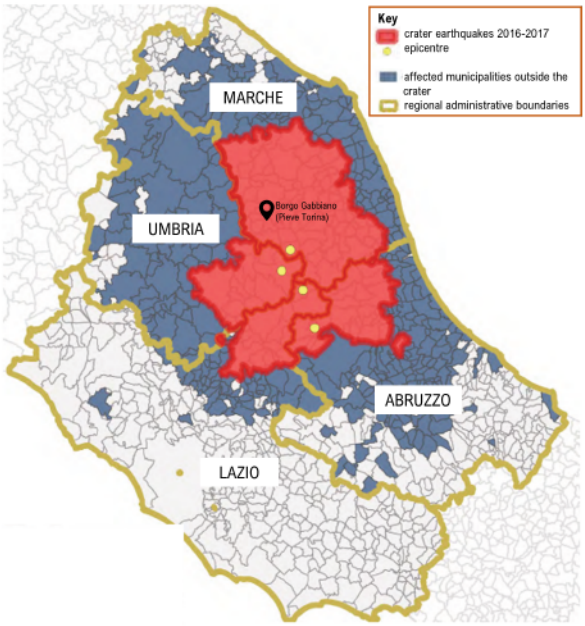

Figure 3.17: Map of the seismic crater in central Italy after earthquakes 2016—2017 (source: report curated by Ufficio Speciale Ricostruzione, January 2020) and identification of the site of interest Gabbiano (Pieve Torina, Italy).

the 2012 Emilia earthquake and therefore became not only de facto but also an official reference tool for the expeditious survey of damages, the definition of damage, the definition of emergency measures and the post-seismic assessment of ordinary buildings [75].

This technical data sheet is used to provide an assessment of the building's condition state and is composed of 8 sections which are structured as follows:

1. Building identification. In this section the building is found by its geographical coordinates and cadastral information. Moreover, a map of the structural aggregate is required and the building identification.

2. Building description. Floor numbers, average floor height, average square meters for each floor, approximate date of construction , type of use etc. are required in section 2.

3. Structural typology. Description of vertical structural parts and horizontal structural parts.

4. Damage to structural elements and emergency measures already carried out. This section must include the level of damage for each structural

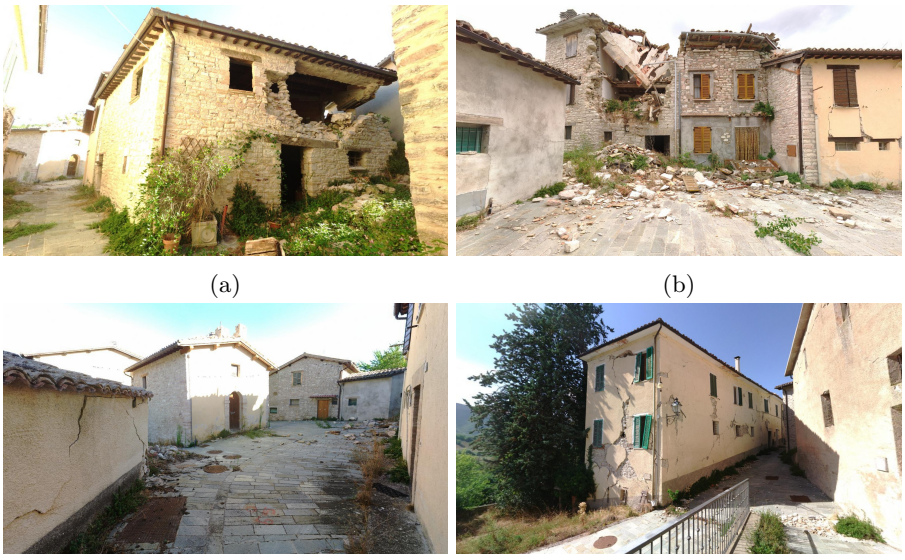

(a) (b)

(c) (d)

Figure 3.18: Damaged buildings in Gabbiano (Pieve Torina, Italy) on which is possible to observe different typologies of collapse. (**a**) Example of collapses stone Façade, (**b**) example of roof collapsed in stone buildings, (**c**) example of small urban area with cracks and (**d**) example of more recent building with cracks.

element and which kind of measures has already been taken.

5. Damage to non-structural elements and emergency measures already carried out.

6. External hazard due to other constructions, networks, slopes and emergency measures carried out.

7. Soil and foundation. In this sections must be reported if there are slopes and damages to foundation.

8. Assessment of accessibility. By assessing the risks, the technician should be able to decide if the building is accessible or not.

As can be seen, all this data is entered through an on-site visual inspection by qualified operators. It is mostly non-metric data, but some of this required information can be documented with the support of geomatics tools and collected to create mappings on information systems such as GIS.

3.2.3 Data acquisition and processing

As it was stated in the previous section, part of the parameters used by the AeDES methodology implies the necessity of having geometrical data (i.e. measurements) of the buildings. In accordance with that, this work proposes an efficient strategy for virtualizing the village by using the approaches suggested by the European preventive conservation project HeritageCARE [77], namely:

1. photogrammetry with UAV for the digitisation of building roofs;
2. terrestrial laser scanning and spherical images for the digitisation of the vertical envelop of the buildings.

All these methodologies are complemented by the use of GNSS points in order to georeference the obtained products. For the GNSS survey, a *"Zenith35 Pro TAG"* from GeoMax was used to acquire the coordinates of 10 points on roads and outdoor pavements, to be used as Ground Control Points (GCP), in about $15 minutes$ (Figure 3.19). In RTK (Real Time Kinematic) mode, the receiver has a horizontal accuracy of $8\ mm \pm 1\ ppm$ (rms) and a vertical accuracy of $15\ mm \pm 1\ ppm$ (rms) [78]. All the points captured by the GNSS were placed in the coordinate system WGS 84 / UTM zone 33N (EPSG:32633).

The aerial photogrammetry was carried out by using the same *"SR-SF6"* VTOL UAV by Skyrobotic [53] with the Sony *"DSC-QX100"* camera mounted as payload as described in Section 3.1.1. This camera is equipped with a $13.37 \times 8.91\ mm$ sensor with 20.2 $MPix$ [54] and a lens with a focal length setting of 10.4 mm. Using the Skydirector app [53], the flight of the UAV was planned to execute 7 photogrammetric strips in nadiral direction at progressive altitudes following the course of the terrain, which presented a difference in height of about 30 m, to maintain a distance of at least 50 m from the objects to be surveyed, with 65% overlap and 60% side lap on an area of about 30 000 m^2 (Figure 3.20). A total of 108 aerial photos were captured, covering the whole area of the survey and the 10 reference points. The average GSD of this flight was about 1.54 cm and the time spent for this flight was about 14 $minutes$.

The photos acquired during the aerial photogrammetric survey were processed by using the same Structure from Motion approach described in Section 3.1.1 [55], allowing us to obtain a 3D point cloud model and an orthophoto of the surveyed area. The inner orientation of the camera was carried out by using a self-calibration approach, considering a Fraser camera model (Table 3.2) [56] and the external orientation of the cameras was performed by using the self-calibration approach as well as a bundle adjustment. During this stage the coordinates of the GNSS points were used as Ground Control Points (GCP). As a result, a photogrammetric model with an RMS error of 4.82 cm was obtained (Table 3.3). Then, a Semiglobal Matching stage was performed

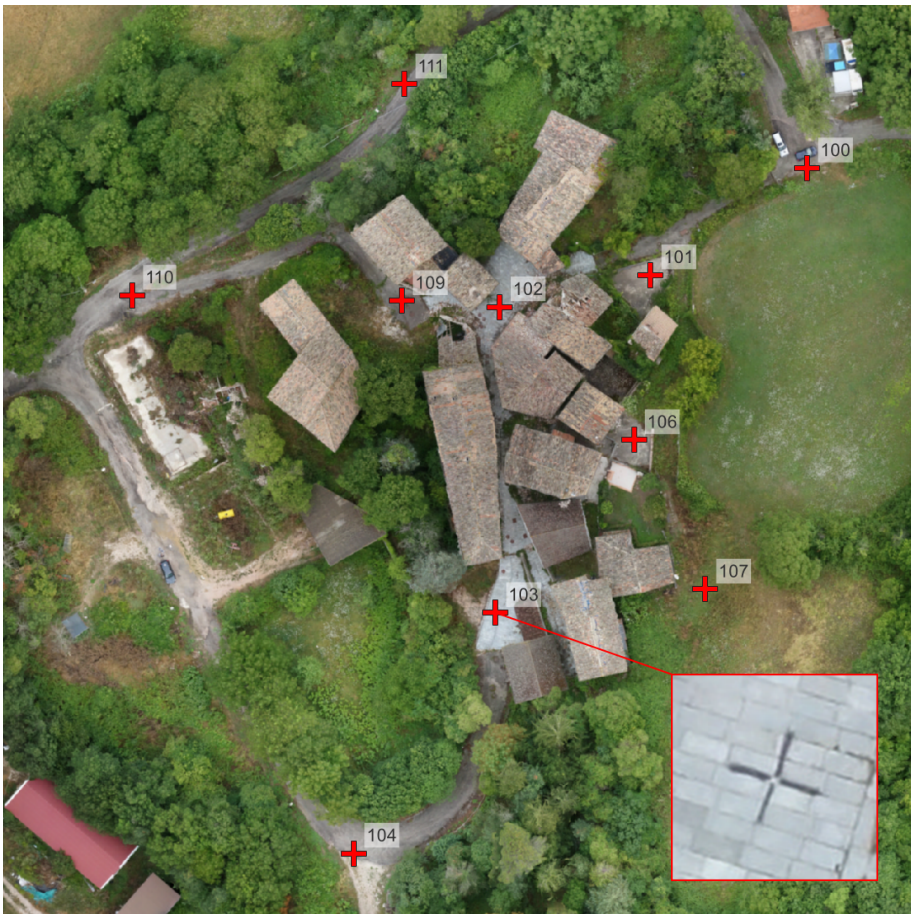

Figure 3.19: Ground Control Point example.

with the aim of obtaining the dense point cloud [57]. This point cloud was made up by 75 027 126 points, allowing to obtain a true orthophoto with a GSD of 1.54 *cm* (Figure 3.21). The total processing time of this phase was about 3*hours* and 30*minutes*.

Table 3.2: Inner parameters of the camera before and after the self-calibration.

Parameter	**Initial value**	**Calibrated value**
Focal length (mm)	10.40	Data
Format size (*height* × *width*) (mm)	13.37 × 8.91	13.37 × 8.91
Principal point (X/Y) (px)	0/0	−17.61/20.59
K1 value (mm^{-2})	0	$6.3 \cdot 10^{-3}$
K2 value (mm^{-4})	0	$-3.3 \cdot 10^{-3}$
P1 value (mm^{-1})	0	$-8.2 \cdot 10^{-4}$
P2 value (mm^{-1})	0	$8.4 \cdot 10^{-4}$

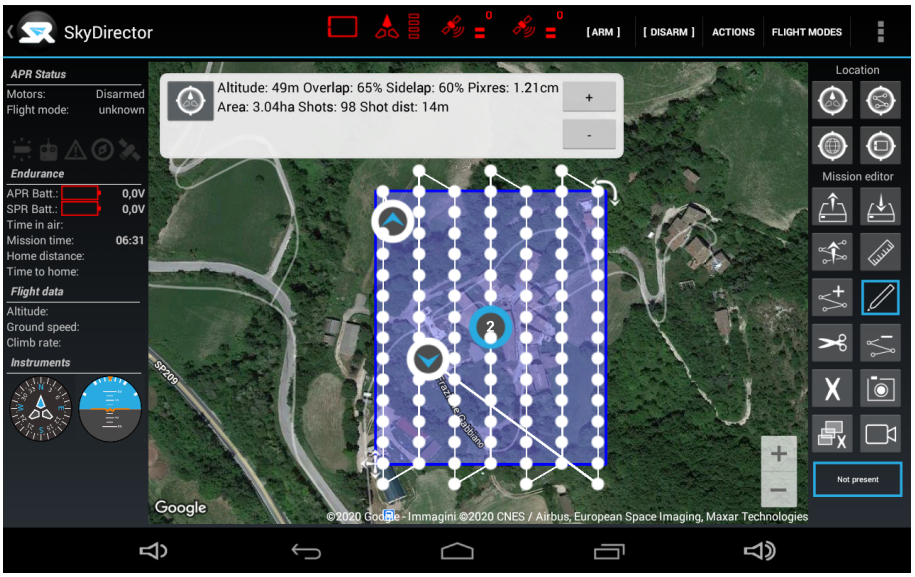

Figure 3.20: SkyDirector app used for UAV flight plan.

Table 3.3: GCP residual errors (X – Easting, Y – Northing, Z – Altitude, Image – Reprojection Error).

Point	X error (cm)	Y error (cm)	Z error (cm)	Total (cm)	Image (pix)
100	-0.81	-0.46	1.99	2.19	0.158
101	2.41	-3.56	4.82	6.46	0.258
102	1.74	-6.22	0.27	6.47	0.463
103	0.86	1.61	0.83	2.01	0.309
104	1.16	-1.05	-1.47	2.15	0.191
106	-0.77	1.79	-0.72	2.07	0.200
107	-1.37	1.88	-1.41	2.72	0.164
109	-2.57	1.66	-2.25	3.80	0.418
110	-0.20	0.29	5.58	5.59	0.240
111	-0.37	3.99	-7.89	8.85	0.198
Total	1.44	2.84	3.62	4.82	0.284

On the other hand, the terrestrial digitisation of the buildings was performed by using the light-weight laser scanner Faro Focus^s 70. This laser scanner is based on the phase shift physical principle with a measurement range from 0.6 to 70 m, a capture rate from 122 000 to 976 000 points per second and a nominal accuracy of 1 mm at 25 m in normal conditions of illumination and reflectivity. A total of 151 scans along the streets of the village, for a total acquisition campaign of about 3 days in an area of about 10 000 m^2, were required in order to obtain a full 3D point cloud of the site (Figure 3.22).

All the scan stations were registered in a local coordinate system by using the Iterative Closest Point (ICP) algorithm [79], obtaining a 3D point cloud

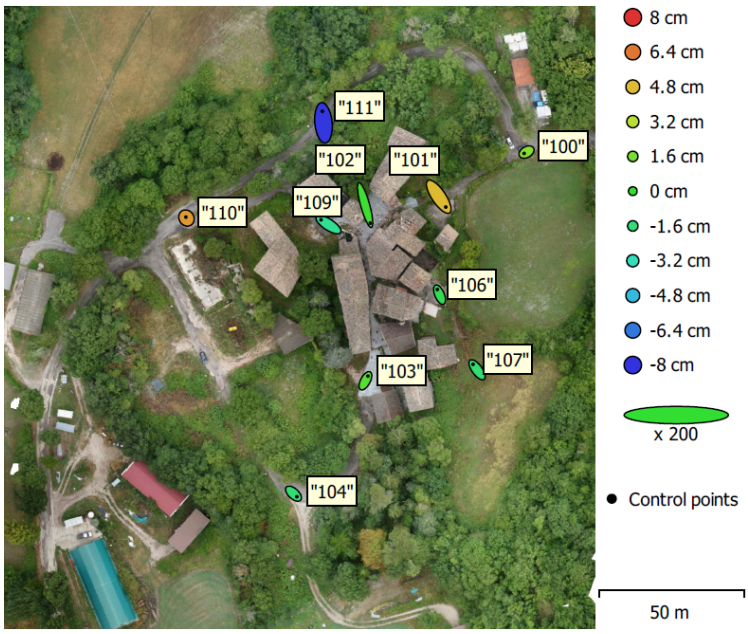

Figure 3.21: Orthophoto of the surveyed area with GCP locations, Z error represented by ellipse color and X,Y errors represented by ellipse shape.

made up by 673 355 488 points. (Figure 3.23). In parallel to each scan, it was captured a spherical image by using the integrated camera of the laser scanner. This image allows us to colorize the point cloud as well as to create a simple virtual environment to support the on-site inspection (Figure 3.22). The 3D point cloud obtained by the laser scanner was georeferenced with the GNSS points by using a 6 parameter Helmert transformation, which resulted in an RMS of 6.82 *cm* (Table 3.4). The whole processing of the LIDAR scans required approximately one day.

Table 3.4: Residual error of the reference points in the terrestrial LIDAR survey.

Point	**Residual Error (cm)**
101	9.45
102	6.25
103	4.70
104	9.08
106	3.81
107	2.75
109	9.85
110	4.55

Figure 3.22: 360° images linked in QGIS.

The point cloud from the aerial photogrammetric survey was then exported and combined with the point cloud from the terrestrial LIDAR survey, resulting in a unified point cloud of 748 362 614 points (Figure 3.24). Using the Cloud Compare software, the Digital Terrain Model (DTM) and the Digital Surface Model (DSM) in raster format were generated from the unified point cloud. These data will be used for the computation of the buildings' parameters explained in Section 3.2.4.

3.2.4 Data integration and management

Since the aim of this work is to develop a pipeline for helping an expedited seismic evaluation at urban scale, only the exterior of the village was surveyed. Also, many of the buildings were severely damaged by the last seismic events in the area and it was not possible to access safely to their interior.

The idea is to satisfy the demand for a complete model by collecting and linking all geometric and non-geometric data in a geo-database. In this case, the open-source software Quantum GIS (QGIS) was used.

The data collected into QGIS were:

Figure 3.23: Point cloud obtained from the terrestrial LIDAR survey (top view).

(a) (b)

Figure 3.24: Unified point cloud: (**a**) Aerial view and (**b**) Street view.

- orthophoto as a raster layer;
- DSM (Digital Surface Model) as a raster layer;
- DTM (Digital Terrain Model) as a raster layer;
- Building contours as a vectorial polygon layers;
- AeDES sheets as a table with no geometry data;
- Spherical images from LiDAR scans as a vectorial points layer;
- Unified point cloud (currently implemented only for visualization purposes).

This software allowed us to develop Python scripts to both improve the user experience and allow the automatic extraction of some parameters concerning the characteristics of the buildings.

Some of these layers are related to each other simply by spatial coordinates and reference systems (raster and vectorial layers with geometry data), while other data are linked via table attributes.

For instance, the AeDES datasheets are related to the buildings with both tables containing the fields "Sheets" and "Parcels", with the possibility that a single AeDES sheet may relate to multiple parcels and that multiple AeDES sheets may have been produced for a parcel during the life of the building. Therefore, a function has been implemented using a script, which allows to filter the AeDES table by selecting a building in the map or in the building's table. This filter will show the AeDES sheets with the same sheet and at least one of the parcels of the selected building. Then to open the file of each AeDES sheet (usually in PDF format) from the table, a simple QGIS action was implemented.

Similarly, for 360° images has been implemented a Python script to allow to open them using an external viewer, by simply clicking on them on the map or in their table. In this case the viewer used is the open-source software FSP viewer [80].

The different information sources captured during the digitisation campaign allow us to automatise the computation of four parameters that are often used, together with other input parameters, for performing expeditive seismic vulnerability assessments. This represents only a starting point, future work may attempt to automate the calculation of the other necessary parameters. A crucial aspect is that the developed Python script, freely available [2], work in any kind of urban scenario, obviously assuming that the validity of these parameters for the seismic assessment depends on the constructive typology of the buildings. These parameters are:

1. number of floors of each building;

2. shape regularity in plan;

3. planimetric position of the building in relation to the cluster;

4. presence of adjacent buildings with different heights in the cluster, in relation to the examined building.

[2] The developed Python script is available in Zenodo at `https://doi.org/10.5281/zenodo.6398968` and in GitHub at `https://github.com/FabioPiccinini/pyvulnerability`

Number of floors

The first of the parameters extracted is the number of floors in each building. Using the raster layers (orthophoto, DTM and DSM), it is simply estimated through the following steps.

1. Extraction of the median of the DSM values and the minimum of the DTM values, falling within the contours of each building. This can be done thanks to the QGIS "zonal statistics" algorithm, which, for each zone of a polygonal vector layer, can perform different statistics about the values of the pixels of a raster layer lying in that zone.

2. Calculation of the the floor number as the difference between DSM median and DTM minimum, divided by the expected floor height and approximated to the nearest integer.

Shape regularity in plan

The second parameter is the shape regularity in plan. The script checks that two of the conditions prescribed by NTC 2018 [81] (Norme Tecniche per le Costruzioni, the Italian Technical Regulations for Construction) for regularity in plan (Paragraph 7.2.1) are checked (Figure 3.25).

1. The contour of the building is convex or the areas between the contour and the circumscribed convex line are less than 5% of the contour area.

2. The ratio of the sides of the rectangle circumscribed around the contour of the building is < 4.

(a) (b)

Figure 3.25: Shape regularity in plan conditions: (**a**) Convex hull in blue. Red area $< 5\%$ of green area. (**b**) Minimum circumscribed rectangle in blue. Ratio of the rectangle sides < 4.

To verify these conditions, the script uses only the contours of the buildings (vectorial polygon layer) and, exploiting the QGIS "convex hull" and "oriented

minimum bounding box" algorithms, creates the polygons described by the two conditions respectively and checks them.

Planimetric position into the cluster

The two remaining parameters concern the clustered buildings only. One is the planimetric position of the building in relation to the cluster ("Center", "Angle" or "End", Figure 3.26). Using only the building contour layer, it is computed for each building with the following steps.

1. Identification of adjacent buildings exploiting the selection rule "extract by location". This rule creates a new vector layer that only contains features from the first vectorial input layer, that matches the selected relative position conditions with regard to the features of the second vectorial input layer. It is worth to mention that if there are not buildings adjacent to the examined one, the script move on to the next building without performing further processing.
2. Computation of the centroid of the examined building using the QGIS algorithm with the same name. The centroid is the barycentre of the polygon.
3. Extraction of the boundaries of the examined building and the adjacent ones, using the QGIS "boundary" algorithm, which transform the polygon layers in polylines layer.
4. Identification of the common boundaries between the examined building and the adjacent ones, exploiting the QGIS "intersection" algorithms which, in the case of two layers of polylines as input, returns only the overlapping polylines as output.
5. Separation of the contact segments through the QGIS algorithm "explode lines", which allow to divide the polylines of the common boundaries into single lines.
6. Examination of each contact segment to establish its contact direction and its validity. The contact direction is perpendicular to the segment, towards the examined building. The validity is based on the position of the centroid of the examined building in relation to the contact segment. The contact segment is valid if the centroid lies on the side facing the examined building and is between the perpendicular lines passing through the start and end of the segment).
7. Recovery of pairs of segments with similar contact directions (within a certain tolerance) for which the centroid was on the side facing the examined building but not between the mentioned perpendicular lines. The

pair of segments is recovered if the centroid was on different sides with respect to the lines perpendicular to the two segments. In this case the average of the two contact directions is considered valid.

8. Computation of the maximum angle difference between all possible pairs of valid contact directions ($\leq 180°$).

9. Determination of the plan position of the building in the cluster based on the calculated maximum angle difference. "Center" if angle $>$ (180° - tolerance), "Angle" if (180° - tolerance) $\geq$ angle $>$ (90° - tolerance) or "End" if (90° - tolerance) $\geq$ angle.

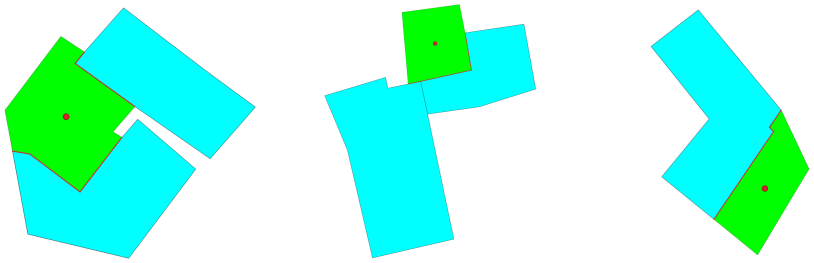

(a) (b) (c)

Figure 3.26: Examples of planimetric positions into the cluster: (**a**) "Center", (**b**) "Angle", (**c**) "End". Examined building in green, adjacent buildings in cyan, centroid as a red point, contact segments as red lines.

Presence of adjacent buildings with different heights

The last parameter determines whether there are buildings with a different height adjacent to the one under examination, considering a certain tolerance (Figure 3.27). The script uses the building contour layer and the DSM layer to determine it with the following steps.

1. Same steps 1, 3, 4 and 5 (skipping step 2) as for the previous parameter in Section 3.2.4, to extract the contact segments with the adjacent buildings.

2. Creation of two buffers for each segment, one on the side of the examined building and one on the side of the adjacent building, exploiting the QGIS algorithm "single sided buffer", which extrude the lines of the input layer for a selected distance towards the chosen side, and return a polygonal vectorial layer.

3. Calculation of the two medians of the DSM values falling into the two buffers, exploiting the same "zonal statistics" algorithm described in the step 1 of Section 3.2.4.

4. If the difference between the two medians is too great, considering a certain tolerance, for at least one contact segment, it means that there are buildings with a different height.

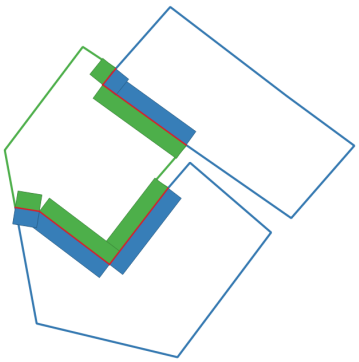

Figure 3.27: Determination of the presence of adjacent buildings with different heights: examined building as a green line, adjacent buildings as blue lines, contact segments as red lines, buffer towards the examined building as green zones and buffer towards the adjacent buildings as blue zones.

Chapter 4

Results

This chapter will present, for each domain of application, the results obtained testing the methodology with the related case study.

4.1 GIS for operation and maintenance of PV systems

Regarding the application domain of operation and maintenance of photovoltaic systems, results from the developed GIS-based system lie in the possibility of creating a complete, customisable and interactive map of photovoltaic systems, such as the one in Figure 4.1, that illustrates the positions of the inverters and switchboards and indicates which inverter the modules are connected to using different colors (Plant B).

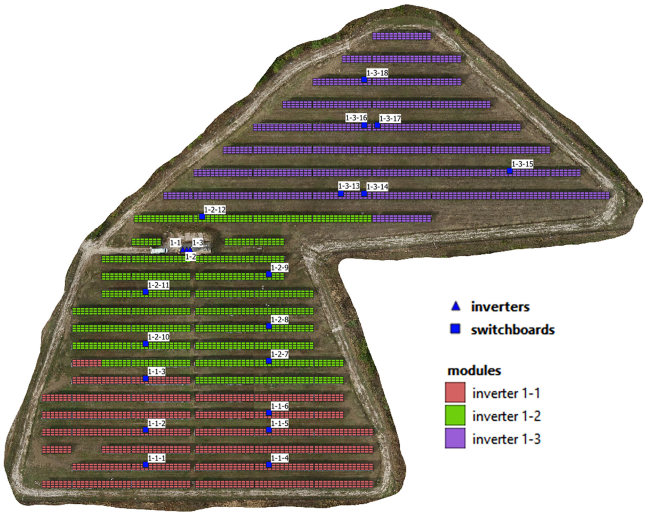

Figure 4.1: The customised map of a PV system that illustrates the positions of the inverters and switchboards and indicates which inverter the modules are connected to using different colors. (Plant B).

For the PV inspection, the thermal images have been collected according to the maintenance plans. The developed database stores successfully the inspection campaigns executed. In fact, it has been applied with success on the previously cited PV plant on the rooftop of an industrial building, in the province of Cuneo (Italy) (Plant A), proving that it can be easily queried, filtered and themed as desired, to represent the needed information in the best possible way. For example, to highlight overheated components resulting from a thermal inspection, as shown in Figure 4.2.

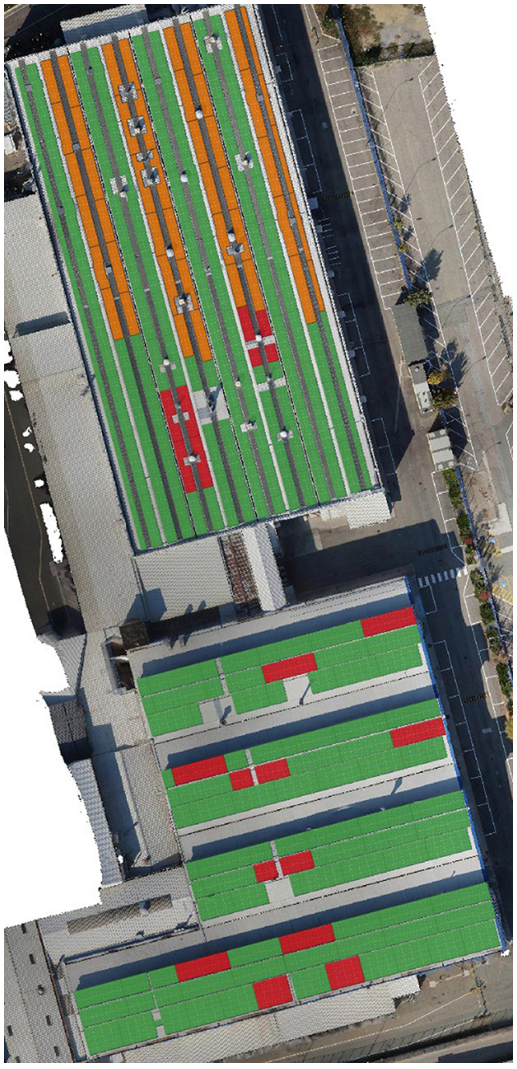

Figure 4.2: The themed map of a PV system to highlight totally overheated strings (in red) and totally overheated arrays (in orange). (Plant A).

From the performed inspection (Plant A) it was found that the fault modules were 915 out of the 3 156 installed overall — i.e., 28.99 % — and in many cases, there were entire malfunctioning strings or arrays.

In QGIS, for selecting the necessary information from time to time, thematic reports could be drafted. A personalized report page could be generated for each selected geometry belonging to a specific layer, such as the ones from the inspection results, using the *"atlas"* function. Figure 4.3 shows a report generated by selecting the features in the *"thermal_inspections_strings"* table which are labeled as entirely overheated, through the *"id_string_defect_type"* field, and generating an *"atlas"* page with: a map zoomed in to the specific geometry which the page is dedicated, and general orthophoto of the PV plant with the objective feature highlighted (Plant A). It could be easily personalized with all the useful information required from the database.

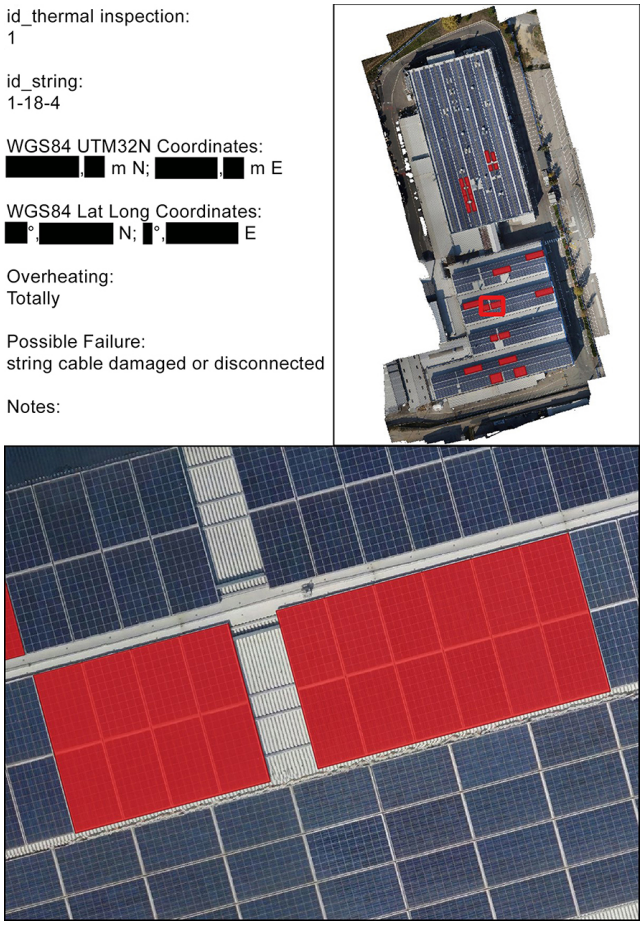

Figure 4.3: Example of a report page generated using the atlas function of QGIS. (Plant A).

In this other example of map customization in Figure 4.4, the spatial distribution of the results of the I–V curve tests, performed on the strings, is shown (Plant B). To generate this map, the features of the *"iv_curve_strings_tests"* layer were coloured by applying a green gradient, depending on the values contained in the *"P_percentage_deviation"* field, assigning a more intense green to the strings that passed the test better. In this case, all the strings had passed the test, otherwise the same could have been done with a red gradient to identify which strings had failed the test more severely than the others. Note that there are no I–V curve tests for strings that are not displayed.

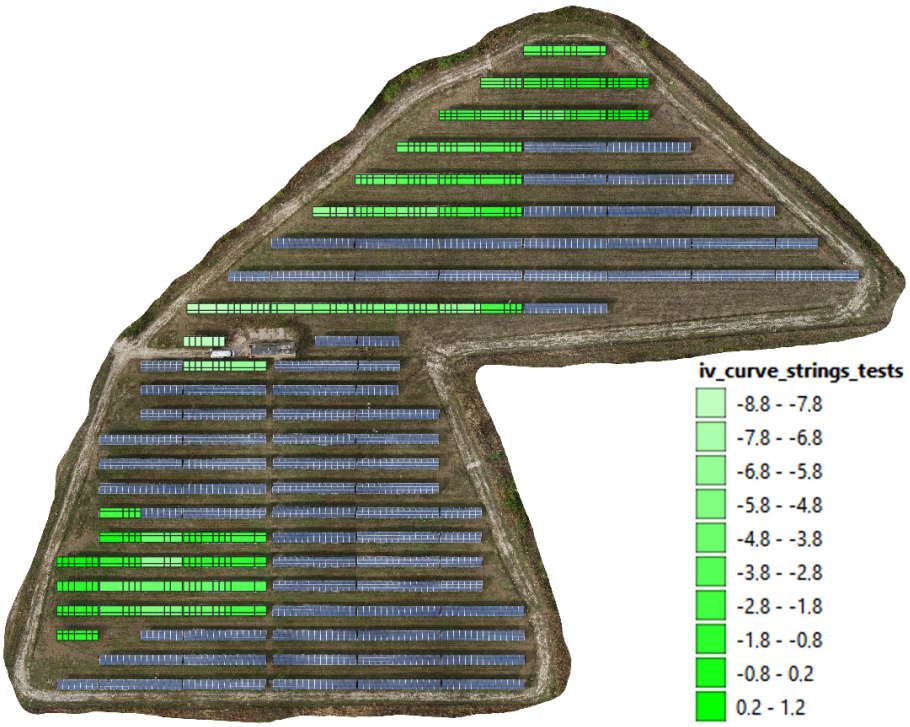

Figure 4.4: The customized map of a PV system to show the results of the I–V curve tests. (Plant B).

To create tables and graphs in QGIS report layouts, it is necessary to use the official plugin called "Data Plotly" [82].

In the example in Figure 4.5, the data regarding the performance ratio check results (Plant B) have been simply extracted from the GIS in table form.

To generate this table, the *"performance_ratio_inverters_checks"* layer features containing the *"id_performance_ratio_checking_campaign"* of the specific check campaign were selected.

The last example of a report obtainable from the GIS concerns the energy

id_inverter	p_dcr	performance_ratio	check result
1-1	330.6	0.886	OK
1-2	330.6	0.861	OK
1-3	335.6	0.906	OK

Figure 4.5: The table with the results of the performance ratio check. (Plant B).

production data of the PV plant. In particular, Figure 4.6 shows a histogram related to the monthly energy production of the Plant B.

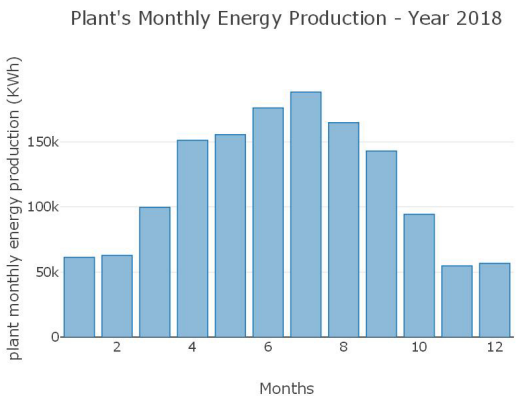

Month	Plant Monthly Energy Production
1	61,341
2	62,833
3	99,687
4	151,146
5	155,435
6	175,944
7	188,125
8	164,633
9	142,881
10	94,342
11	54,753
12	56,742

Figure 4.6: The histogram and table with the monthly energy production data (Plant B).

This was generated by selecting the features of the *"plants_monthly_energy_production"* layer with the value of the specific year in the *"plant_production_year"* field, setting the values of the *"plant_production_month"* field as the x-axis, and the values of the *"plant_monthly_energy_production"* field as the y-axis.

4.1.1 Automatic Faults Detection with Deep Learning Algorithm

In this Section, the results of the experiments conducted on the photovoltaic thermal images dataset are reported. In particular, two experiments were performed: the first one is based on the performance comparison of the three image segmentation networks (U-Net, LinkNet and FPN) and the second one involves the Mask R-CNN for the instance segmentation task. Finally, a comparative analysis of the networks is carried out. The photovoltaic thermal

images dataset was split into three subset: 70% for training, 20% for validation and 10% for the final test. For both image and instance segmentation, the evaluation metrics used were the Dice and Jaccard indexes.

In the first experiment, the performances of three image segmentation networks were compared. The results achieved by these networks are summarized in Table 4.1 in terms of the Jaccard and Dice indexes. Results show that all networks showed good performance and are very similar: LinkNet slightly outperformed the others in terms of Jaccard index while U-Net was better than the others in terms of the Dice index.

Table 4.1: Evaluation of image segmentation on photovoltaic thermal images test set by using U-Net, LinkNet and FPN networks.

	Jaccard	**Dice**
U-Net	0.741	**0.841**
LinkNet	**0.748**	0.825
FPN	0.734	0.825

For the second experiment, we trained and tested the Mask R-CNN network. In contrast to other DNNs, this network has been specifically developed for instance segmentation.

The training was performed in three steps:

- Network trained from scratch;
- Network pretrained on the Microsoft Common Objects in the Context dataset (MS-COCO) [83], then retraining all layers;
- Network pretrained on the MS-COCO dataset, then retraining only the layers of the head section (the classifier section).

The technique of retraining a pre-trained network on another dataset is a transfer learning technique called fine tuning, and it is widely adopted in cases of small datasets. This technique generally allows to train a network faster than training from scratch.

Another difference compared to other networks is that it obtaines as output a mask for each anomalous predicted cell. For obtaining Jaccard and Dice metrics, a post-processing phase is needed to combine all the masks of the instances into a single overall mask. Table 4.2 reports the Instance segmentation results on the photovoltaic thermal images test set by using a Mask-RCNN network. The results of the three training approaches are reported, in terms of Jaccard and Dice metrics.

Table 4.2: Instance segmentation results on the photovoltaic thermal images test set by using a Mask-RCNN network.

	Jaccard	**Dice**
Mask-RCNN (all)	0.382	0.493
Mask-RCNN (pretrain-all)	0.106	0.175
Mask-RCNN (pretrain-head)	**0.499**	**0.605**

The results show that using a pre-trained network and re-training only the head part allows obtaining a good instance segmentation network: it achieved 0.499 on the Jaccard index and 0.605 on the Dice index. These performances are higher than the network trained from scratch. The tests also show that totally re-training a pre-trained network could lead to worse results than training it from scratch.

Finally, Table 4.3 presents a comparative analysis of the performance of the best networks for both segmentation approaches. The trainable parameters and the training time are also reported. For this comparison, the chosen networks are U-Net, for its Jaccard and Dice index metrics, and Mask RCNN pre-trained on the MS-COCO dataset and re-trained only on the the head part. The results reveal that the U-Net outperformed the other approaches. However, Mask-RCNN has the key advantage that it directly outputs the position of each single predicted cell. Conversely, U-Net outputs a single overall mask, but through a post-processing step based on image processing techniques, it can be easily split into the individual predicted cells.

Table 4.3: Comparative analysis of the performance of the best networks for both segmentation approaches.

	Jaccard	**Dice**	**Trainable Params**	**Total Params**	**Training Time**	**Test Time**
U-Net	**0.741**	**0.841**	74.7 Million	75 Million	192 s/epoch	15 ms
Mask-RCNN	0.499	0.605	21 Million	44.6 Million	212 s/epoch	24 ms

Figure 4.7 allows a visual analysis of the results obtained by the U-Net network on the test set. It represents some examples of test images, their ground truth and the relative predicted mask. Figure 4.7c shows that the network may have false positives in the predicted mask, i.e., some areas are misclassified as anomalous cells. These false positives usually have a very small area.

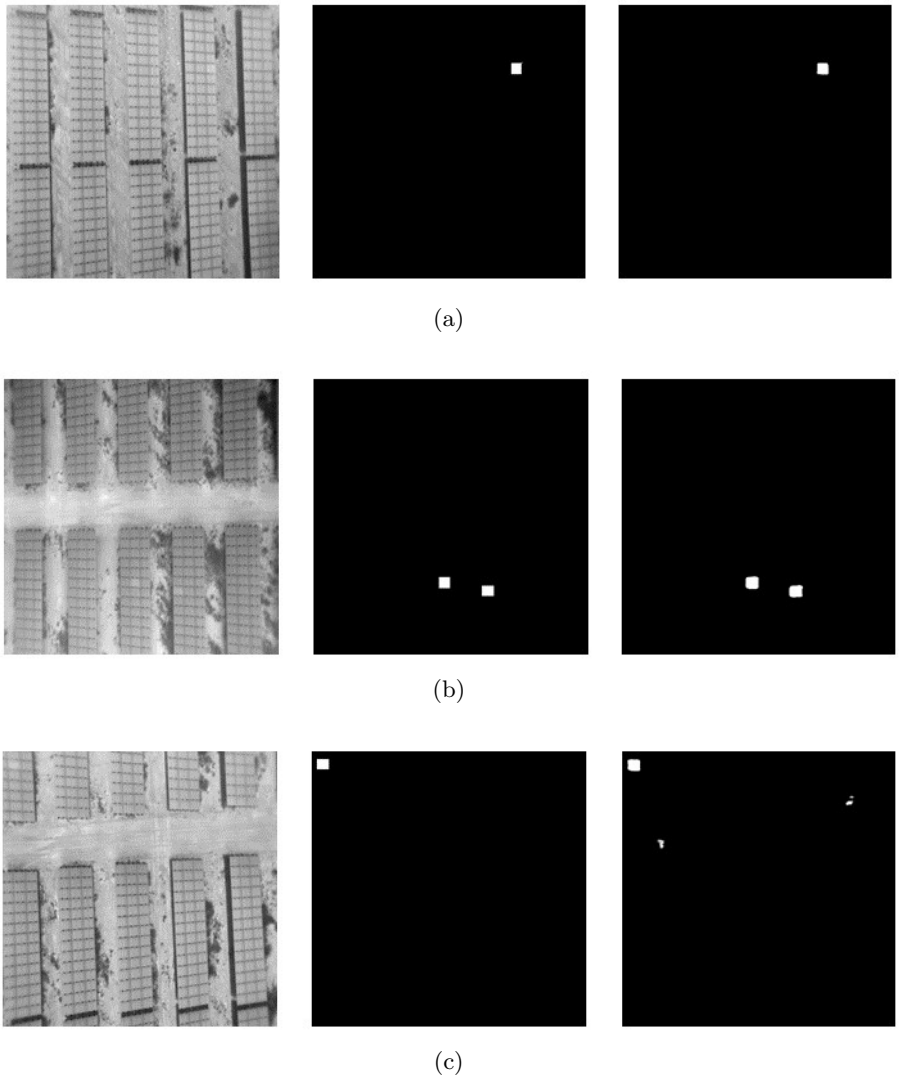

(a)

(b)

(c)

Figure 4.7: U-Net performance on test set images, with ground truth and predicted mask. The masks of (**a**,**b**) have been correctly predicted. (**c**) depicts some misclassified areas.

4.2 Urban survey data integration and management in GIS

With regard to urban surveys, results from the developed QGIS framework are illustrated in this section. In particular, in Section 4.2.1 the integration within the GIS of all the data previously described will be illustrated, while Sec-

tion 4.2.2 will present the results of the geometric parameters of the buildings that have been automatically extracted using the developed Python script, that is openly available in Zenodo at `https://doi.org/10.5281/zenodo.6398968` and in GitHub at `https://github.com/FabioPiccinini/pyvulnerability`

4.2.1 Integration of information

As it was stated in Section 3.2.4, the QGIS framework developed by this work should be able to integrate different type of information (i.e. raster, vectorial, 3D point clouds and 360º images) (Figure 4.8).

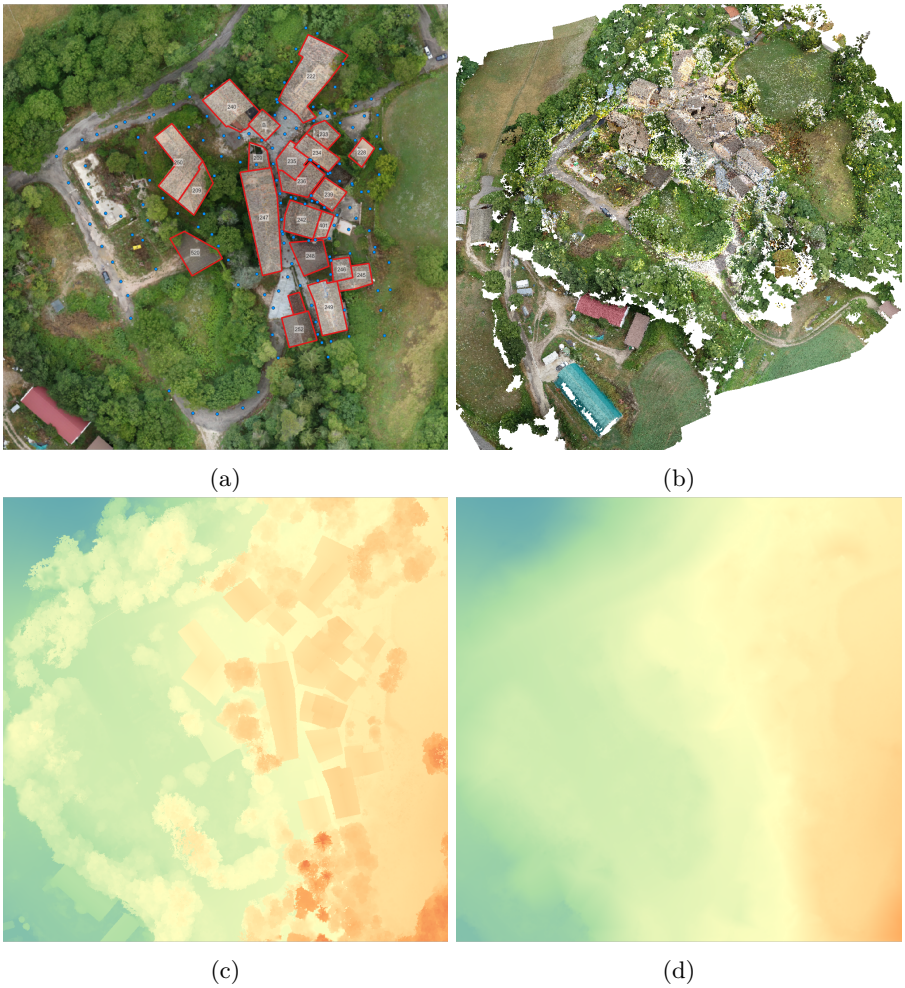

(a) (b)

(c) (d)

Figure 4.8: Data in QGIS: (**a**) Polygons of buildings and points of 360° images on the orthophoto; (**b**) Point cloud visualisation in a 3D map; (**c**) DSM and (**d**) DTM, with a spectral false colour scale.

The raster information was directly imported into the platform. The first information source was the orthophoto created through the aerial photogrammetry. 360º images were introduced into the QGIS project as a point vectorial layer, stored in a shapefile, visible above the aerial orthophoto. This shapefile has direct links to each panorama. Thanks to this, if the user wants to virtually consult one building it can be done by just clicking on the point, the project will run FSP viewer to open the associated panorama. This type of information allows to evaluate the type of collapse mechanism of the building as well as the different constructive solution adopted during its construction. Figure 3.18a shows an example of collapsed building made up by a two-leaf masonry wall with a timber structure. At the first floor the building shows some iron ties that prevent the out-of-plane deformation of part of the structure. However, the upper part of the structure has collapse due to the formation of an out-of-plane mechanism. Concerning the 3D point cloud, in the current version of QGIS (3.22) only its visualisation in both 2D and 3D map is supported (Figure 4.8b).

Additionally to this geometrical information, the geo-spatial database links each building with its associated AeDES sheet (Figure 4.9). The table displays the files path and, thanks to a simple QGIS action, it's possible to open them with the O.S. default application.

AEDES Sheets :: Elementi Totali: 16, Filtrati: 16, Selezionati: 0

	id	Azioni	Date	Sheet	Parcels	File
1	NULL	Open File	2016-09-25	52	['247']	.\AEDES\PDF\2016-09-25_F52_P247.pdf
2	NULL	Open File	2016-09-25	52	['251']	.\AEDES\PDF\2016-09-25_F52_P251.pdf
3	NULL	Open File	2016-09-25	52	['415']	.\AEDES\PDF\2016-09-25_F52_P415.pdf
4	NULL	Open File	2016-09-25	52	['463']	.\AEDES\PDF\2016-09-25_F52_P463.pdf
5	NULL	Open File	2018-02-20	52	['245', '246']	.\AEDES\PDF\2018-02-20_F52_P245-246.pdf
6	NULL	Open File	2018-03-01	52	['234']	.\AEDES\PDF\2018-03-01_F52_P234.pdf
7	NULL	Open File	2018-03-01	52	['236']	.\AEDES\PDF\2018-03-01_F52_P236.pdf
8	NULL	Open File	2018-03-01	52	['247']	.\AEDES\PDF\2018-03-01_F52_P247.pdf
9	NULL	Open File	2018-03-01	52	['248']	.\AEDES\PDF\2018-03-01_F52_P248.pdf
10	NULL	Open File	2018-03-17	52	['222']	.\AEDES\PDF\2018-03-17_F52_P222.pdf
11	NULL	Open File	2018-03-17	52	['233']	.\AEDES\PDF\2018-03-17_F52_P233.pdf
12	NULL	Open File	2018-03-19	52	['249']	.\AEDES\PDF\2018-03-19_F52_P249.pdf
13	NULL	Open File	2018-03-20	52	['240']	.\AEDES\PDF\2018-03-20_F52_P240.pdf
14	NULL	Open File	2018-03-20	52	['250']	.\AEDES\PDF\2018-03-20_F52_P250.pdf
15	NULL	Open File	2018-03-20	52	['252']	.\AEDES\PDF\2018-03-20_F52_P252.pdf
16	NULL	Open File	NULL	52	['235']	.\AEDES\PDF\nodata_F52_P235.pdf

Mostra Tutti gli Elementi

Figure 4.9: Attribute table of the AeDES sheets.

The office work was complemented by the app QField [84], allowing to edit and manage the different shapefiles of the project by using an Android smartphone or tablet (Figure 4.10). This application could be used in field with the aim of improving the work carried out by the technicians.

4.2.2 Automatic extraction of parameters

Once all the geometrical data was uploaded to the QGIS platform it was possible to automatically calculate the four geometrical parameters defined in Section 3.2.4. All these parameters are stored within the geo-spatial database as is shown in Figure 4.11.

As mentioned in section 3.2.4, the process to extract the first parameter also automatically computes the median value of the DSM and the minimum value of the DTM for each building and store them in the attribute table, as can be seen in Figure 4.11. The output of the floor parameter calculation is shown by the thematic map in Figure 4.12a.

The results of the second parameter, concerning the shape regularity in plan of the building, are displayed by the thematic map in Figure 4.12b. There are 7 buildings out of 22 with no regularity in shape. These buildings are coloured in red, while all the buildings which fulfils the geometrical conditions for shape regularity from the Italian regulation NTC 2018 [81] are coloured in green.

Another parameter extracted, useful for studying the vulnerability of a building is the planimetric position of the building related to its adjacent buildings. The classification shows four different scenarios, classified as "center", "angle", "end" and "isolated" building. The algorithm calculates how the buildings must be classified so in the thematic map in Figure 4.12c they are visible respectively in green, yellow, red and cyan colour, highlighting how they are classified. Apart from the 5 "isolated" buildings, only one is classified as "center" and one is classified as "angle". All the others are considered as "end" in their respective cluster.

The last parameter automatically calculated concerned the adjacent building height difference. Two pairs of buildings have a considerable difference in height. They are all displayed with the letter Y (yes) in the attribute table and in red colour in the dedicated thematic map in Figure 4.12d. All the 13 buildings in green may be considered with almost no height difference. The 5 isolated buildings, in cyan, cannot be considered in this calculation as there are no adjacent buildings to be compared with.

(a) (b)

(c) (d)

Figure 4.10: Screenshots of the QField application with the data generated inside the QGIS project: (**a**) General view of the cadastral layer, the ortophoto and the point layer that represents the different scan stations; (**b**) View of the project tree; (**c**) Appearance of the app when the user consult the data contained in a shapefile and (**d**) Appearance of the app when the user edits a field.

Buildings :: Elementi Totali: 22, Filtrati: 22, Selezionati: 0

	Azioni	Sheet	Parcels	Floors	ShapePIReg	PlanLoc	DifHeight	DSM_median	DTM_min
1	Filter building's AEDES sheets	52	222	2	N	NULL	NULL	713,6733398437...	706,5580810546...
2	Filter building's AEDES sheets	52	233	3	Y	E	N	716,5554809570...	708,5056017645...
3	Filter building's AEDES sheets	52	228	2	Y	NULL	NULL	715,3580322265...	710,4609784807...
4	Filter building's AEDES sheets	52	239	2	Y	NULL	NULL	714,8875427246...	709,5052858923...
5	Filter building's AEDES sheets	52	242	3	Y	E	N	716,0350952148...	706,6243552183...
6	Filter building's AEDES sheets	52	250	3	N	E	N	710,0805053710...	700,6599440801...
7	Filter building's AEDES sheets	52	520	2	Y	NULL	NULL	703,5634765625...	697,2479248046...
8	Filter building's AEDES sheets	52	247	4	Y	E	Y	714,0994873046...	703,4891321518...
9	Filter building's AEDES sheets	52	209	1	Y	E	Y	710,2274780273...	705,8944325166...
10	Filter building's AEDES sheets	52	B	2	Y	E	N	712,7280883789...	707,0968287733...
11	Filter building's AEDES sheets	52	240	3	Y	E	N	713,7515258789...	703,6807971191...
12	Filter building's AEDES sheets	52	248	3	Y	NULL	NULL	713,3184814453...	705,6960144042...
13	Filter building's AEDES sheets	52	246	2	Y	A	N	714,7245483398...	709,1184414950...
14	Filter building's AEDES sheets	52	249	3	N	E	N	716,5039672851...	706,4945252300...
15	Filter building's AEDES sheets	52	252	3	Y	E	Y	711,4498291015...	703,2897261362...
16	Filter building's AEDES sheets	52	NULL	1	Y	E	Y	707,0205078125...	704,2940572102...
17	Filter building's AEDES sheets	52	209	3	N	E	N	709,1325073242...	700,7650909423...
18	Filter building's AEDES sheets	52	234	2	Y	E	N	715,5015258789...	708,8630371093...
19	Filter building's AEDES sheets	52	235	2	N	C	N	714,5554809570...	707,9679679361...
20	Filter building's AEDES sheets	52	236	2	N	E	N	713,8850708007...	707,5958958675...
21	Filter building's AEDES sheets	52	401	2	Y	E	N	716,1044921875...	709,1866295083...
22	Filter building's AEDES sheets	52	245	2	N	E	N	715,1962890625...	709,9693297823...

Mostra Tutti gli Elementi

Figure 4.11: Attribute table of the buildings, showing the calculated parameters.

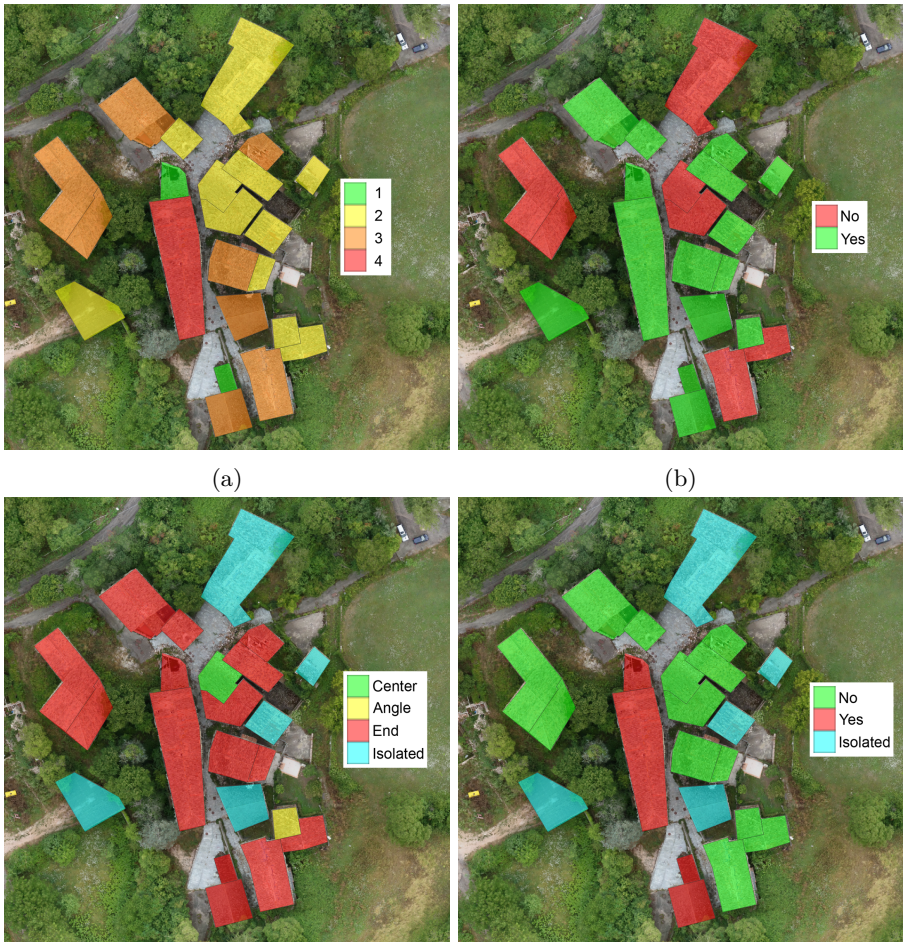

(a) (b)

(c) (d)

Figure 4.12: Thematic maps of the 4 extracted parameters of the buildings, shown in QGIS: (**a**) Number of floors (**b**) Shape regularity in plan (**c**) Planimetric location in the cluster (**d**) Presence of adjacent buildings with different height.

Chapter 5

Discussion

The integration of the use of GIS into the pipeline of case studies treated for the two application domains brought several benefits that will be discussed in this chapter.

Regarding PV plants thermographic inspections and management in GIS, the developed relational conceptual model has potential applicability for the O&M of PV farms, since it facilitates the management of heterogeneous data in a unique database. It thus underpins several advantages that are worth being discussed.

First of all, the solution is open-source, whereas it is current practice to adopt black-box commercial solutions that are not designed to be adapted and customised for every need as this system is. Moreover, the developed relational database is a powerful instrument for PV plant management, thanks to the great possibilities of data analysis and the ease of the production of thematic reports provided by GIS, rather than conducting them manually or with other instruments such as CAD. The use of this maintenance system is especially useful for large power plants, where the management becomes very difficult using traditional methods.

Given that thermal inspections proved to be a very valid method for the health check, the proposed GIS management system will provide a full analysis of the faults evolution through time and space, allowing us to assess the impact of the faulty modules on the undamaged ones. Perhaps it could also help to study new innovative predictive and preventive maintenance systems in the future.

As described in Section 3.1.1, overheated components detection requires the visual analysis of each individual thermal image by an operator, to manually identify thermal anomalies. However, the new artificial intelligence UAV-based inspection system introduced in Section 3.1.1, when tested on the dataset we provided, confirmed its effectiveness and suitability to the diagnosing of thermal images of PV plants. In particular, the networks chosen obtained high values on the Jaccard and Dice indices. This approach for defect analysis can be an essential aid to assist operators for O&M operations, reducing cost and errors

arising from manual operations [66]. Considering that, nowadays, inspections are entrusted to visual inspections, our approach will both reduce the overall costs of PV module maintenance and increase the efficiency of PV plants. The output results of the proposed experiments can be easily integrated within a dedicated geographical information system (GIS) specifically designed for operation and maintenance (O&M) activities in PV Plants. Indeed, having the geolocation for each image, the management of the detected faulty cells can be facilitated.

As demonstrated by the two case studies presented, the system is designed to handle electrical data, allowing to keep track of the efficiency of the PV plant. By merging all data in a GIS solution, managers can plan maintenance over time.

Concerning instead the urban surveys with photogrammetry and TLS, this work aims at improving the methodology presented by Indirli et al. [51, 52] for the integration of the AeDES inspection forms (used for quick post-seismic evaluations) into a GIS framework. These improvements were the following ones:

- the use of additional geomatic tools;
- the automation of the computation of some of the parameters concerning the geometrical characteristics of the buildings;
- the use of the QField app for improving the in-field work of the technicians.

About the first one, in this work aerial photogrammetry (Structure from Motion and UAV) has been used for the generation of aerial ortophotos as well as for capturing the information of the roofs. Then the 3D point cloud generated by the aerial photogrammetry has been integrated with the TLS point cloud, allowing to obtain a complete digitisation of the village. Additionally, has been introduced the use of 360º images as a quick virtual resource for evaluating the collapse mechanism and construction system of the buildings. This virtual resource is integrated directly into the QGIS platform allowing to load directly the 360º image by means of the FSP viewer. This digitisation required a total time of about four days.

Concerning the second improvement, several Python scripts that calculates in an automatic way four different parameters have been developed, enhancing the performance of the traditional AeDES approach.

Finally, the use of the QField app, which allow to modify and manage all the information in-situ, has been proposed. This aspect is considered critical since the AeDES approach is mainly based on visual inspection in field.

Chapter 6

Conclusions and future works

In this thesis the use of GIS was introduced in the two application domains about PV plants monitoring and management and about urban surveys with advanced geomatic techniques.

Chapter 1 provided a description of the context that motivated the realisation of this thesis and its main objectives and contributions.

Chapter 2 illustrated the state of the art regarding the use of GIS in the two application domains.

Chapter 3 described the followed pipelines with their respective data acquisition and processing steps, detailing the structure of the relational geodatabase for the management of photovoltaic systems and the algorithms written in Python for the automatic computation of parameters concerning the geometric characteristics of buildings, while presenting the case studies used to test them.

Chapter 4 presented the results obtained following the described procedures, which were then discussed in Chapter 5.

This chapter aims to highlight some possible improvements and future developments that could build on this work.

For instance, the geodatabase for the management of photovoltaic plants could be interconnected with the Automatic Fault Detection systems for the automatic storage and analysis of all the provided results, perhaps by exploiting the possibility of writing custom scripts with Python. New Automatic Fault Detection systems will also probably be developed in the future and could be tested by exploiting the dataset made available to download for research purposes by this work [1] [66].

In addition, given the open source nature of the developed solution, the structure of the developed geodatabase, available for download [2] [1], can be expanded to store other types of data that were not initially planned to be included. For future works, an important task could be to collect more in-

[1] PV thermal images dataset download link: `http://vrai.dii.univpm.it/content/photovoltaic-thermal-images-dataset`

[2] PV GIS database conceptual model download link: `http://www.mdpi.com/1996-1073/13/11/2860/s1`

formation from different PV plants and to attempt a predictive maintenance approach based on the collected data.

Regarding GIS for the integration of data from urban surveys, this work focused on the extraction of geometric parameters useful for the assessment of seismic vulnerability, developing a Python script made freely available [3], but the same approach can be extended to other architectural or engineering purposes, calculating different types of parameters.

As a concluding remark, it is worth to note that the proposed methodology fulfils with the European SENDAI framework for disaster risk reduction [85] in at least two of four basic principles: i) Understanding disaster risk and iv) enhancing disaster preparedness for effective response, and to "Build Back Better" in recovery, rehabilitation and reconstruction. This is not trivial, and the introduction of Geomatic integrated survey as a current practice for increasing the knowledge of villages represents a fundamental step forward. The combined use of panoramic images, terrestrial laser scanning and aerial photogrammetry, by means of the structure from motion approach, proves to be the best combination in terms of efficiency/data acquired.

Future works could be focused on the development of new algorithms for the automatic extraction of additional geometrical parameters and the use of the geometrical data for generating simplified BIM (Building Information Modeling) models.

Moreover, the automatic extraction of geometrical parameters could be improved by exploiting the 3D point cloud obtained by the TLS. In this sense, it could be used the RANSAC (RANdom SAmple Consensus) Shape Detector approach [86] for extracting the different vertical walls and roof planes. Then this segmentation could be compared with the original planes, allowing to evaluate the presence of out-of-plane mechanism as well as deflections of the structure. This segmentation could be used for generating BIM models with simplified geometry that allow technicians to manage the interventions as well as to create numerical models for evaluating the seismic response of the structures. The latter will allow to create a complete managing tool integrating GIS and BIM technologies for the post-seismic assessment.

In conclusion, in the future both application domains could benefit from the continued development of mixed reality systems. For PV systems, technicians could benefit from augmented reality visors that could assist them in field operations by providing information from the developed geodatabase and also allowing to update this information in real time. While for urban surveys, the same concept could be exploited with augmented reality to provide and update information on buildings, or sub-services that can be added in the GIS, but also

[3] The developed Python script is available in Zenodo at `https://doi.org/10.5281/zenodo.6398968` and in GitHub at `https://github.com/FabioPiccinini/pyvulnerability`

virtual reality to explore the model and linked information in an immersive way from the comfort of the office.

Bibliography

[1] F. Piccinini, R. Pierdicca, and E. S. Malinverni, "A relational conceptual model in gis for the management of photovoltaic systems," *Energies*, vol. 13, no. 11, 2020. [Online]. Available: https://www.mdpi.com/1996-1073/13/11/2860

[2] B. Resch, G. Sagl, T. Törnros, A. Bachmaier, J.-B. Eggers, S. Herkel, S. Narmsara, and H. Gündra, "Gis-based planning and modeling for renewable energy: Challenges and future research avenues," *ISPRS International Journal of Geo-Information*, vol. 3, no. 2, pp. 662–692, 2014. [Online]. Available: https://www.mdpi.com/2220-9964/3/2/662

[3] H. Bagan and Y. Yamagata, "Analysis of urban growth and estimating population density using satellite images of nighttime lights and land-use and population data," *GIScience & Remote Sensing*, vol. 52, no. 6, pp. 765–780, 2015. [Online]. Available: https://doi.org/10.1080/15481603.2015.1072400

[4] S. Abdullahi, B. Pradhan, S. Mansor, and A. R. M. Shariff, "Gis-based modeling for the spatial measurement and evaluation of mixed land use development for a compact city," *GIScience & Remote Sensing*, vol. 52, no. 1, pp. 18–39, 2015. [Online]. Available: https://doi.org/10.1080/15481603.2014.993854

[5] E. S. Malinverni, R. Pierdicca, F. Colosi, and R. Orazi, "Dissemination in archaeology: a gis-based storymap for chan chan," *Journal of Cultural Heritage Management and Sustainable Development*, vol. 9, no. 4, pp. 500–519, 2019.

[6] A. Agrillo, V. Surace, P. Liberatore, and L. Benedetti, "Rapporto delle attività 2018 del gestore dei servizi energetici," Gestore dei Servizi Energetici, GSE, Tech. Rep., may 2019, available online. [Online]. Available: https://www.gse.it/

[7] X. Li, Q. Yang, Z. Lou, and W. Yan, "Deep learning based module defect analysis for large-scale photovoltaic farms," *IEEE Transactions on Energy Conversion*, vol. 34, no. 1, pp. 520–529, 2019.

[8] S. Gorjian, B. N. Zadeh, L. Eltrop, R. R. Shamshiri, and Y. Amanlou, "Solar photovoltaic power generation in iran: Development, policies, and barriers," *Renewable and Sustainable Energy Reviews*, vol. 106, pp. 110–123, 2019. [Online]. Available: https://www.sciencedirect.com/science/article/pii/S1364032119301182

[9] J. Ascencio-Vásquez, I. Kaaya, K. Brecl, K.-A. Weiss, and M. Topič, "Global climate data processing and mapping of degradation mechanisms and degradation rates of pv modules," *Energies*, vol. 12, no. 24, 2019. [Online]. Available: https://www.mdpi.com/1996-1073/12/24/4749

[10] V. Sharma and S. Chandel, "Performance and degradation analysis for long term reliability of solar photovoltaic systems: A review," *Renewable and Sustainable Energy Reviews*, vol. 27, pp. 753–767, 2013. [Online]. Available: https://www.sciencedirect.com/science/article/pii/S1364032113004917

[11] J. A. Tsanakas, L. Ha, and C. Buerhop, "Faults and infrared thermographic diagnosis in operating c-si photovoltaic modules: A review of research and future challenges," *Renewable and Sustainable Energy Reviews*, vol. 62, pp. 695–709, 2016. [Online]. Available: https://www.sciencedirect.com/science/article/pii/S1364032116301629

[12] R. Pierdicca, E. S. Malinverni, F. Piccinini, M. Paolanti, A. Felicetti, and P. Zingaretti, "Deep convolutional neural network for automatic detection of damaged photovoltaic cells," *The International Archives of the Photogrammetry, Remote Sensing and Spatial Information Sciences*, vol. XLII-2, pp. 893–900, 2018. [Online]. Available: https://www.int-arch-photogramm-remote-sens-spatial-inf-sci.net/XLII-2/893/2018/

[13] F. Grimaccia, S. Leva, A. Dolara, and M. Aghaei, "Survey on pv modules' common faults after an o amp;m flight extensive campaign over different plants in italy," *IEEE Journal of Photovoltaics*, vol. 7, no. 3, pp. 810–816, 2017.

[14] T. Nam and T. A. Pardo, "Smart city as urban innovation: Focusing on management, policy, and context," in *Proceedings of the 5th International Conference on Theory and Practice of Electronic Governance*, ser. ICEGOV '11. New York, NY, USA: Association for Computing Machinery, 2011, p. 185–194. [Online]. Available: https://doi.org/10.1145/2072069.2072100

[15] T. Vinodkumar, *Geographic information system for smart cities*. Copal Publishing Group, 2016.

[16] F. D. Stefano, A. Gorreja, F. Piccinini, R. Pierdicca, and E. S. Malinverni, "3d gis for a smart management system applied to historical villages damaged by earthquake," in *Proceedings ARQUEOLÓGICA 2.0 - 9th International Congress & 3rd GEORES - GEOmatics and pREServation*, 2021.

[17] A. Almeida, L. Gonçalves, A. Falcão, and S. Ildefonso, "3d-gis heritage city model: case study of the historical city of leiria," *AGILE 2016, Helsinki*, pp. 14–17, 2016.

[18] E. Lenticchia and E. Coïsson, "The use of gis for the application of the phenomenological approach to the seismic risk analysis: The case of the italian fortified architecture," *The International Archives of the Photogrammetry, Remote Sensing and Spatial Information Sciences*, vol. XLII-5/W1, pp. 39–46, 2017. [Online]. Available: https://www.int-arch-photogramm-remote-sens-spatial-inf-sci.net/XLII-5-W1/39/2017/

[19] K. Poljanšek, A. Casajus, and M. M. F. Valles, "Recommendations for national risk assessment for disaster risk management in eu," 2019.

[20] A. Gastli and Y. Charabi, "Solar electricity prospects in oman using gis-based solar radiation maps," *Renewable and Sustainable Energy Reviews*, vol. 14, no. 2, pp. 790–797, 2010. [Online]. Available: https://www.sciencedirect.com/science/article/pii/S1364032109002196

[21] M. de Simón-Martín, A.-M. Diez-Suárez, L.-Á. de Prado, A. González-Martínez, A. De La Puente-Gil, and J. Blanes-Peiró, "Degradation monitoring of photovoltaic plants: Advanced gis applications," *Solar Panels and Photovoltaic Materials; IntechOpen: London, UK*, p. 93, 2018.

[22] M. De Simón-Martín, A.-M. Diez-Suárez, L. Álvarez-de Prado, A. González-Martínez, Á. De la Puente-Gil, and J. Blanes-Peiró, "Development of a gis tool for high precision pv degradation monitoring and supervision: Feasibility analysis in large and small pv plants," *Sustainability*, vol. 9, no. 6, 2017. [Online]. Available: https://www.mdpi.com/2071-1050/9/6/965

[23] J. Tsanakas, D. Chrysostomou, P. Botsaris, and A. Gasteratos, "Fault diagnosis of photovoltaic modules through image processing and canny edge detection on field thermographic measurements," *International Journal of Sustainable Energy*, vol. 34, no. 6, pp. 351–372, 2015. [Online]. Available: https://doi.org/10.1080/14786451.2013.826223

[24] A. Shiota, G. Fuchino, Y. Koyamatsu, Y. Kakumoto, K. Tanoue, Y. Qudaih, and Y. Mitani, "Guide construction of an efficient inspection, maintenance and asset management of photovoltaic power generation system using gis," *Energy Procedia*, vol. 100, pp. 69–77, 2016, 3rd International Conference on Power and Energy Systems Engineering, CPESE 2016, 8-10 September 2016, Kitakyushu, Japan. [Online]. Available: https://www.sciencedirect.com/science/article/pii/S1876610216310943

[25] A. Shiota, Y. Koyamatsu, K. Fuji, Y. Mitani, and Y. Qudaih, "Development and public release of solar radiation map for effective use of solar energy based on gis with digital surface model," *system*, vol. 2, p. 4, 2015.

[26] M. Brumenm, N. Lukac, and B. Zalik, "Gis application for solar potential estimation on buildings roofs," *IARIA WEB*, 2015.

[27] A. Verso, A. Martin, J. Amador, and J. Dominguez, "Gis-based method to evaluate the photovoltaic potential in the urban environments: The particular case of miraflores de la sierra," *Solar Energy*, vol. 117, pp. 236–245, 2015. [Online]. Available: https://www.sciencedirect.com/science/article/pii/S0038092X15002066

[28] M. Victoria and G. B. Andresen, "Using validated reanalysis data to investigate the impact of the pv system configurations at high penetration levels in european countries," *Progress in Photovoltaics: Research and Applications*, vol. 27, no. 7, pp. 576–592, 2019. [Online]. Available: https://onlinelibrary.wiley.com/doi/abs/10.1002/pip.3126

[29] H. Yousefi, H. Hafeznia, and A. Yousefi-Sahzabi, "Spatial site selection for solar power plants using a gis-based boolean-fuzzy logic model: A case study of markazi province, iran," *Energies*, vol. 11, no. 7, 2018. [Online]. Available: https://www.mdpi.com/1996-1073/11/7/1648

[30] E. Noorollahi, D. Fadai, M. Akbarpour Shirazi, and S. H. Ghodsipour, "Land suitability analysis for solar farms exploitation using gis and fuzzy analytic hierarchy process (fahp)—a case study of iran," *Energies*, vol. 9, no. 8, 2016. [Online]. Available: https://www.mdpi.com/1996-1073/9/8/643

[31] T. Huld, R. Müller, and A. Gambardella, "A new solar radiation database for estimating pv performance in europe and africa," *Solar Energy*, vol. 86, no. 6, pp. 1803–1815, 2012. [Online]. Available: https://www.sciencedirect.com/science/article/pii/S0038092X12001119

[32] E. Malinverni, S. Chiappini, and R. Pierdicca, "A geodatabase for multi-source data management applied to cultural heritage: The case study of villa buonaccorsi's historical garden," *The International Archives of Photogrammetry, Remote Sensing and Spatial Information Sciences*, vol. 42, pp. 771–776, 2019.

[33] L. Rossi, A. Ajmar, M. Paolanti, and R. Pierdicca, "Vehicle trajectory prediction and generation using lstm models and gans," *Plos one*, vol. 16, no. 7, p. e0253868, 2021.

[34] X. Li, Z. Lv, J. Hu, B. Zhang, L. Yin, C. Zhong, W. Wang, and S. Feng, "Traffic management and forecasting system based on 3d gis," in *2015 15th IEEE/ACM International Symposium on Cluster, Cloud and Grid Computing*, 2015, pp. 991–998.

[35] S. Chiappini, A. Fini, E. Malinverni, E. Frontoni, G. Racioppi, and R. Pierdicca, "Cost effective spherical photogrammetry: a novel framework for the smart management of complex urban environments," *The International Archives of Photogrammetry, Remote Sensing and Spatial Information Sciences*, vol. 43, pp. 441–448, 2020.

[36] L. J. Sánchez-Aparicio, M.-G. Masciotta, J. García-Alvarez, L. F. Ramos, D. V. Oliveira, J. A. Martín-Jiménez, D. González-Aguilera, and P. Monteiro, "Web-gis approach to preventive conservation of heritage buildings," *Automation in Construction*, vol. 118, p. 103304, 2020. [Online]. Available: https://www.sciencedirect.com/science/article/pii/S0926580520306749

[37] T. M. Ferreira, R. Vicente, J. A. Raimundo Mendes da Silva, H. Varum, A. Costa, and R. Maio, "Urban fire risk: Evaluation and emergency planning," *Journal of Cultural Heritage*, vol. 20, pp. 739–745, 2016, cultural HELP 2014 Special Issue. [Online]. Available: https://www.sciencedirect.com/science/article/pii/S1296207416300577

[38] P. Ortiz, V. Antunez, J. M. Martín, R. Ortiz, M. A. Vázquez, and E. Galán, "Approach to environmental risk analysis for the main monuments in a historical city," *Journal of Cultural Heritage*, vol. 15, no. 4, pp. 432–440, 2014. [Online]. Available: https://www.sciencedirect.com/science/article/pii/S1296207413001635

[39] R. Ortiz, P. Ortiz, M. Vázquez, and J. Martín, "Integration of georeferenced informed system and digital image analysis to asses the effect of cars pollution on historical buildings," *Construction and Building Materials*, vol. 139, pp. 320–333, 2017. [Online]. Available: https://www.sciencedirect.com/science/article/pii/S0950061817302155

[40] A. Saha, S. C. Pal, M. Santosh, S. Janizadeh, I. Chowdhuri, A. Norouzi, P. Roy, and R. Chakrabortty, "Modelling multi-hazard threats to cultural heritage sites and environmental sustainability: The present and future scenarios," *Journal of Cleaner Production*, vol. 320, p. 128713, 2021. [Online]. Available: https://www.sciencedirect.com/science/article/pii/S0959652621029127

[41] A. Gonzalez, A. Basaglia, E. Spacone, and G. Brando, "A qgis plugin for the seismic vulnerability assessment of urban centers: Application to the city of popoli in abruzzo (italy)," in *Proceedings of the 12th International Conference on Structural Analysis of Historical Constructions*. SAHC, 09 2021.

[42] N. S. Sauti, M. E. Daud, M. Kaamin, and S. Sahat, "Gis spatial modelling for seismic risk assessment based on exposure, resilience, and capacity indicators to seismic hazard: a case study of pahang, malaysia," *Geomatics, Natural Hazards and Risk*, vol. 12, no. 1, pp. 1948–1972, 2021. [Online]. Available: https://doi.org/10.1080/19475705.2021.1947903

[43] F. Rezaie and M. Panahi, "Gis modeling of seismic vulnerability of residential fabrics considering geotechnical, structural, social and physical distance indicators in tehran using multi-criteria decision-making techniques," *Natural Hazards and Earth System Sciences*, vol. 15, no. 3, pp. 461–474, 2015.

[44] S. Karimzadeh, M. Miyajima, R. Hassanzadeh, R. Amiraslanzadeh, and B. Kamel, "A gis-based seismic hazard, building vulnerability and human loss assessment for the earthquake scenario in tabriz," *Soil Dynamics and Earthquake Engineering*, vol. 66, pp. 263–280, 2014.

[45] M. Vettore, M. Donà, P. Carpanese, V. Follador, F. da Porto, and M. R. Valluzzi, "A multilevel procedure at urban scale to assess the vulnerability and the exposure of residential masonry buildings: The case study of pordenone, northeast italy," *Heritage*, vol. 3, no. 4, pp. 1433–1468, 2020. [Online]. Available: https://www.mdpi.com/2571-9408/3/4/80

[46] L. G. F. Salazar and T. M. Ferreira, "Seismic vulnerability assessment of historic constructions in the downtown of mexico city," *Sustainability*, vol. 12, no. 3, 2020. [Online]. Available: https://www.mdpi.com/2071-1050/12/3/1276

[47] M. Francini, S. Artese, S. Gaudio, A. Palermo, and M. F. Viapiana, "To support urban emergency planning: A gis instrument for the choice of optimal routes based on seismic hazards," *International Journal of*

Disaster Risk Reduction, vol. 31, pp. 121–134, 2018. [Online]. Available: https://www.sciencedirect.com/science/article/pii/S2212420917303618

[48] F. Romis, S. Caprili, W. Salvatore, T. M. Ferreira, and P. B. Lourenço, "An improved seismic vulnerability assessment approach for historical urban centres: The case study of campi alto di norcia, italy," *Applied Sciences*, vol. 11, no. 2, 2021. [Online]. Available: https://www.mdpi.com/2076-3417/11/2/849

[49] J. Ortega, G. Vasconcelos, H. Rodrigues, and M. Correia, "A vulnerability index formulation for the seismic vulnerability assessment of vernacular architecture," *Engineering Structures*, vol. 197, p. 109381, 2019. [Online]. Available: https://www.sciencedirect.com/science/article/pii/S0141029618342287

[50] R. Vicente, T. Ferreira, R. Maio, H. Varum, A. A. Costa, A. Costa, C. S. Oliveira, and J. M. C. Estêvão, "Seismic vulnerability assessment of existing masonry buildings: case study of the old city centre of faro, portugal," in *2nd European Conference on Earthquake Engineering and Seismology*, 2014, pp. 1–9.

[51] M. Indirli, S. Bruni, E. Candigliota, F. Geremei, F. Immordino, L. Moretti, D. Abate, G. Furini, S. Pierattini, A. Screpanti *et al.*, "Assessment of historic centres through a multidisciplinary approach based on the simultaneous application of remote sensing, gis and quick procedures for survey and vulnerability evaluation: the arsita case," in *5th International Congress" Science and Technology for the Safeguard of Cultural Heritage in the Mediterranean Basin". Istanbul, Turkey, 22nd-25th November*, 2011.

[52] M. Indirli, G. Marghella, A. Marzo, L. Moretti, and A. Formisano, "The proposal of a pre/post-earthquake "holistic & digital" quick survey tool for smart geo-referenced digital building inventories," in *Proc. SE-50 EEE (Skopje Earthquake 50 Years of European Earthquake Engineering) Conference*, 2013.

[53] "Datasheet srsf6 skyrobotic," Available online: http://www.skyrobotic.com/wp-content/uploads/2015/09/Datasheet-SRSF6_Skyrobotic.pdf, (accessed on 06 November 2020).

[54] "Dsc-qx100 specifications," Available online: https://www.sony.co.uk/electronics/support/compact-cameras-dsc-qx-series/dsc-qx100/specifications, (accessed on 06 November 2020).

[55] D. Gonzalez-Aguilera, L. López-Fernández, P. Rodriguez-Gonzalvez, D. Hernandez-Lopez, D. Guerrero, F. Remondino, F. Menna, E. Nocerino,

I. Toschi, A. Ballabeni, and M. Gaiani, "Graphos – open-source software for photogrammetric applications," *The Photogrammetric Record*, vol. 33, no. 161, pp. 11–29, 2018. [Online]. Available: https://onlinelibrary.wiley.com/doi/abs/10.1111/phor.12231

[56] C. Fraser *et al.*, "Multiple focal setting self-calibration of close-range metric cameras," *Photogrammetric Engineering and Remote Sensing*, vol. 46, no. 9, pp. 1161–1171, 1980.

[57] H. Hirschmuller, "Stereo processing by semiglobal matching and mutual information," *IEEE Transactions on Pattern Analysis and Machine Intelligence*, vol. 30, no. 2, pp. 328–341, 2008.

[58] IEC Standard, "60891. photovoltaic devices. procedures for temperature and irradiance corrections to measured iv characteristics," *International Electrotechnical Commission*, 2009.

[59] ——, "Iec 61724-1:2021 international standard. photovoltaic system performance – part 1: Monitoring," *International Electrotechnical Commission*, 2021. [Online]. Available: https://webstore.iec.ch/publication/65561

[60] A. Sangwongwanich, Y. Yang, D. Sera, and F. Blaabjerg, "Lifetime evaluation of grid-connected pv inverters considering panel degradation rates and installation sites," *IEEE Transactions on Power Electronics*, vol. 33, no. 2, pp. 1225–1236, 2018.

[61] S. Lindig, I. Kaaya, K.-A. Weiss, D. Moser, and M. Topic, "Review of statistical and analytical degradation models for photovoltaic modules and systems as well as related improvements," *IEEE Journal of Photovoltaics*, vol. 8, no. 6, pp. 1773–1786, 2018.

[62] F. Grimaccia, S. Leva, and A. Niccolai, "Pv plant digital mapping for modules' defects detection by unmanned aerial vehicles," *IET Renewable Power Generation*, vol. 11, no. 10, pp. 1221–1228, 2017. [Online]. Available: https://ietresearch.onlinelibrary.wiley.com/doi/abs/10.1049/iet-rpg.2016.1041

[63] Z. Xi, Z. Lou, Y. Sun, X. Li, Q. Yang, and W. Yan, "A vision-based inspection strategy for large-scale photovoltaic farms using an autonomous uav," in *2018 17th International Symposium on Distributed Computing and Applications for Business Engineering and Science (DCABES)*, 2018, pp. 200–203.

[64] "Flir tau 2 specifications," Available online: https://www.flir.com/globalassets/imported-assets/document/tau2_product_specification.pdf, (accessed on 15 May 2020).

[65] "Flir e75 specifications," Available online: https://flir.netx.net/file/asset/3910/original, (accessed on 15 May 2020).

[66] R. Pierdicca, M. Paolanti, A. Felicetti, F. Piccinini, and P. Zingaretti, "Automatic faults detection of photovoltaic farms: solair, a deep learning-based system for thermal images," *Energies*, vol. 13, no. 24, 2020. [Online]. Available: https://www.mdpi.com/1996-1073/13/24/6496

[67] M. Tan and Q. Le, "EfficientNet: Rethinking model scaling for convolutional neural networks," in *Proceedings of the 36th International Conference on Machine Learning*, ser. Proceedings of Machine Learning Research, K. Chaudhuri and R. Salakhutdinov, Eds., vol. 97. PMLR, 09–15 Jun 2019, pp. 6105–6114. [Online]. Available: https://proceedings.mlr.press/v97/tan19a.html

[68] O. Ronneberger, P. Fischer, and T. Brox, "U-net: Convolutional networks for biomedical image segmentation," in *Medical Image Computing and Computer-Assisted Intervention – MICCAI 2015*, N. Navab, J. Hornegger, W. M. Wells, and A. F. Frangi, Eds. Cham: Springer International Publishing, 2015, pp. 234–241.

[69] A. Chaurasia and E. Culurciello, "Linknet: Exploiting encoder representations for efficient semantic segmentation," in *2017 IEEE Visual Communications and Image Processing (VCIP)*, 2017, pp. 1–4.

[70] T.-Y. Lin, P. Dollar, R. Girshick, K. He, B. Hariharan, and S. Belongie, "Feature pyramid networks for object detection," in *Proceedings of the IEEE Conference on Computer Vision and Pattern Recognition (CVPR)*, July 2017.

[71] K. He, G. Gkioxari, P. Dollár, and R. Girshick, "Mask r-cnn," in *Proceedings of the IEEE international conference on computer vision*, 2017, pp. 2961–2969.

[72] S. Ren, K. He, R. Girshick, and J. Sun, "Faster r-cnn: Towards real-time object detection with region proposal networks," in *Advances in neural information processing systems*, 2015, pp. 91–99.

[73] A. Jäger-Waldau *et al.*, "Pv status report 2019," *Publications Office of the European Union: Luxembourg*, 2019.

[74] Comitato Elettrotecnico Italiano, "Regola tecnica di riferimento per la connessione di utenti attivi e passivi alle reti at ed mt delle imprese distributrici di energia elettrica," *Tech. Rep. CEI 0-16*, 2014.

[75] C. Baggio, A. Bernardini, R. Colozza, L. Corazza, M. Della Bella, G. Di Pasquale, M. Dolce, A. Goretti, A. Martinelli, G. Orsini *et al.*, "Field manual for post-earthquake damage and safety assessment and short term countermeasures (aedes)," *European Commission—Joint Research Centre—Institute for the Protection and Security of the Citizen, Bruxelles, EUR*, vol. 22868, 2007.

[76] G. Di Pasquale and A. Goretti, "Functional and economic vulnerability of residential buildings affected by recent italian earthquakes," in *X National conference of seismic engineering in Italy, Potenza-Matera*, vol. 913, 2001.

[77] L. Ramos, M. Masciotta, M. J. Morais, M. Azenha, T. Cunha Ferreira, E. Pereira, and P. Lourenco, *HeritageCARE: Preventive conservation of built cultural heritage in the South-West Europe.* CRC Press, 01 2018.

[78] "Geomax zenith35 pro bro 849551 0916 en lr," Available online: https://geomax-positioning.com/-/media/files/geomax/downloads/products/gnss/zenith35/geomaxzenith35probro8495510916enlr.ashx?la=en&hash=12876B33E88473A55C6298DC60C7FFCC, (accessed on 06 November 2020).

[79] P. J. Besl and N. D. McKay, "Method for registration of 3-D shapes," in *Sensor Fusion IV: Control Paradigms and Data Structures*, P. S. Schenker, Ed., vol. 1611, International Society for Optics and Photonics. SPIE, 1992, pp. 586 – 606. [Online]. Available: https://doi.org/10.1117/12.57955

[80] "Fsp viewer," Available online: http://www.fsoft.it/FSPViewer/, (accessed on 26 December 2021).

[81] "Norme tecniche per le costruzioni (ntc2018), ministero delle infrastrutture e dei trasporti: Roma, italy," 2018.

[82] "Data plotly," Available online: https://plugins.qgis.org/plugins/DataPlotly/, (accessed on 15 May 2020).

[83] T.-Y. Lin, M. Maire, S. Belongie, J. Hays, P. Perona, D. Ramanan, P. Dollár, and C. L. Zitnick, "Microsoft coco: Common objects in context," in *European conference on computer vision.* Springer, 2014, pp. 740–755.

[84] "Qfield - efficient field work built for qgis," Available online: https://qfield.org/, (accessed on 28 December 2021).

[85] E. Maly and A. Suppasri, "The sendai framework for disaster risk reduction at five: Lessons from the 2011 great east japan earthquake and tsunami," *International Journal of Disaster Risk Science*, vol. 11, no. 2, pp. 167–178, 2020.

[86] R. Schnabel, R. Wahl, and R. Klein, "Efficient ransac for point-cloud shape detection," *Computer Graphics Forum*, vol. 26, no. 2, pp. 214–226, 2007. [Online]. Available: https://onlinelibrary.wiley.com/doi/abs/10.1111/j.1467-8659.2007.01016.x